LUND UNIVERSITY

A model for immunotherapies against small, solid and motile tumors

Emelie Flood
Department of Astronomy and Theoretical Physics
Lund University
Sweden
In collaboration with
Department of Mathematics
Swinburne University of Technology
Australia

Supervised by Dr. Federico Frascoli and Ass. Prof. Stefan Wallin

Contents

Acknowledgments

I would like to thank the participants of this research project.
Prof. Billy Todd and Swinburne University of Technology for letting me use your excellent resources do my masters project here. A special thanks to Dr. Federico Frascoli for your time, help and support in supervising this project. I would also like to thank Assistant Prof. Stefan Wallin at the department of theoretical physics for your guidance.
I am grateful to the Department of Physics at Lund University for inspiring and educating me during the last five years.

Abstract

Most of all deaths from cancer are due to tumor metastasis, specifically 9 out of 10. Metastasis is associated with a number of factors, including cancer cell motility, tumor adhesive property and cancer shape. As a result, the dynamics, development and consequent prognosis of tumors are still not well characterized.

The development of immunotherapies for cancer has been a focus for research in recent years and a number of studies show that it has great potential as a possible cure against cancer. In simple terms, immunotherapies elicit a specific body's immune response enabling it to prevent diseases. Results indicate that vaccination of 3-5% of cytotoxic T cells in lymph nodes can result in an effective counteraction against cancer development. Also, clinical trials have shown encouraging outcomes, although there are still many factors in the interaction between the immune response and cancer that are not understood.

We present a three dimensional model simulating the interaction between an immune response and motile cancers after a preventative vaccine. Tumor movement is modeled using effective physical forces, with a specific focus on cell-to-cell adhesion properties and tumor cells velocity, thus taking into account the availability of cancer cells to spread and metastasize. Previous studies have pointed out that immunotherapies can be effective against small, solid tumors, but did not consider the possibility of cancer cells detaching from each other and spread. We also investigate the model dependence on the shape, density and distribution of the tumor. This shows some predictive power in determining the outcome of an immune response against solid, small (less than 10 000 cells) tumors. Our results indicate that low tumor velocity is a good indicator for a successful eradication before relapse, whilst metastasis and high velocity leads, almost invariably, to relapse and tumor escape. The effect of cell-to-cell adhesion on prognosis is itself also velocity dependent. Shape measurements have shown to be strongly related to cell distribution in different sized clusters and the probability of a successful eradication of the tumor.

In conclusion, our results generally indicate that some of the measurement techniques available to clinicians for the classification of tumors can bear some predictive power in immunotherapy.

Keywords

Cancer, tumor, agent based model, delay differential equation, immunotherapy, Matlab, computations, CTL, cell motility, adhesion, repulsion, Metropolis algorithm.

1 Introduction

1.1 Background

Cancer is one of the major causes of death in the developed world. The probability of developing invasive cancer through-out a lifetime is 45% for men and 38% for women and its associated mortality rates remains considerably high [1]. This is true in particular for tumors that have the ability to spread through a process known as metastasis. When this event occurs, the tumor cells have the chance to detach from the cancer mass where they grow, and move away from their initial birth site. This often results in an invasion of other organs by cancer cells, with an often fatal outcome for the patient. Example of very aggressive tumors are given, among others, by glioblastomas [2].

The body's defense against diseases is provided by the immune system. Vaccinations can boost the immune system response and favor a strong immune attack against selected external and internal agents and pathogens, thus preventing the onset of diseases. Recently, considerable research has been focused upon developing a vaccine against cancer. An example of an effective vaccine would involve the stimulation of an immune response, in particular the cytotoxic T lymphocytes (CTL) that will recognize the cancer cells, recruit other cells and migrate to the tumor site, attacking and killing the cancer cells [3]. Experiments have been performed that suggest that such a vaccine is a possibility [4, 5]. In these experiments CTLs have been extracted, activated in vivo and injected back into the patients. This led to the onset of the immune response and a reduction of the patients' metastatic melanoma. However, it is difficult to isolate specific parameters in a biological system, and to better understand how a tumor grows and interacts with its surroundings mathematical models have been created to investigate these mechanisms. This has been a major focus of research in both physics and applied mathematics communities and the models have evolved from being based on diffusion equations [6], to more refined approaches involving ordinary and partial differential equations (see [7] and [8] for a review of these). One of the shortcomings of some of these models is that they have been deterministic and one-dimensional. Recently, new models have been developed, and "hybrid" systems in two dimensions have been suggested: e.g. agent based model coupled with differential equations, combining determinism and stochasticity [9, 10].

On the other hand, cellular movement is, in general, not fully understood, even though its causes, character and physical and mathematical attributes have been of interest to researchers for quite a long time [11]. Cells can move both as single cells and as a collective group and their characteristic dynamical and kinematic properties have been analyzed [12]. It is indeed relevant to study the effect of the movement of single cells in the context of tumor growth and immunotherapies. Motility is in fact crucial and is also believed to influence the shape of the tumor [13]. Together with cell-to-cell adhesive properties [14], motility is one of the relevant factors in assessing the malignancy of cancer [15, 16]. For example, previous studies have suggested that a potential therapy can be given by pharmacological agents that block tumor motility [17], whereas research exists for assessing how modified adhesion can aid tumor eradication [18]. For these reasons, in this thesis we investigate how adhesion and motility can affect the outcome of an immune response stimulated by appropriate vaccination against cancers improving on a well-established mathematical model of such process [19]. Although the implementation of a generic and effective vaccine against tumors is still unavailable, immunotherapies do represent a promising technique worth investigating [20].

1.2 Biological background

Tumorigenesis arises from cell mutations that take place in the DNA [21]. Most of these are due to external factors and less than 10% are genetically transferred [22]. However, these mutations are different for different cancers and they can be few or many and may occur earlier or later stages in the tumorigenesis. Many variables exist. The mutations lead to six important alterations in the cell that are all necessary for the development of a tumor. These alterations are: self sufficiency in growth signals, insensitivity to growth inhibitory signals, evasion of programmed cell death, limitless reproduction potential, sustained angiogenesis and tissue invasion and metastasis [23].

When normal cell division occurs, mitogenic growth signals are present and penetrate the cell membrane to bind to signaling molecules. Tumor cells do not show the same dependence on external growth cells as normal cells and it is believed that they can generate their own growth signals. The ability for tumor cells to divide freely is an important difference to normal cells [24].

Tumor cells also have the ability to withstand the external anti-growth signals that the body uses to regulate cell growth. The antigrowth signals govern what state of the cell cycle the cell is in, and is mediated via the retinoblastoma protein. In tumor cells, a disruption of this retinoblastoma protein pathway occurs and the tumor cell can withstand the antigrowth signals [25].

Furthermore, it is important to remark that tumor cells have mutations that inhibit programmed cell death (apoptosis) leading to unlimited cell replication. This is one of the distinct signatures of possibly all cancer types. Apoptosis of a cell is controlled by sensors and effectors: they monitor the intracellular and extracellular environment of the cell for abnormalities and upregulate apoptotic signals [26]. Tumor cells thus acquire the ability of avoiding apoptosis by mutation, and this is primarily through a tumor suppressor gene together with the antiapoptotic pathway [27].

Unfortunately, all previous properties contribute to create limitless replication for the tumor cells, although a final limitation that has to be overcome is the finite replication potential that any normal cell possesses. Once cells divide a certain number of times, they cannot undergo division any more, due to the shortening of the telomeres in each round of the DNA replication. Tumor cells instead activate a special enzyme, telomerase, which maintains the telomeres at a constant length and thereby allows for unlimited division [28].

In order for the tumor to progress to larger sizes it also acquires the capability to encourage blood vessel growth. This is necessary for the tumor to obtain vital nutrition [29]. In this paper the tumor is assumed to be in an early stage when it has not yet achieved this ability and is thus of limited dimensions. Similar assumptions for early stage tumors have been made in a number of other studies, e.g. Mallet et al. [10] and Kim et al. [19].

Note that 90% of all the deaths due to cancer are due to tumor metastasis, the spread of the tumor cells leading to secondary tumor growths [30]. In general, cell-to-cell interactions vary considerably in tumors that lose interaction molecules functioning to suppress movement and metastasis. It is believed that suppression of cell-to-cell adhesion molecules is a major cause of metastasis [31]. This suppression is important during nutrition stress: a fully functioning cell-to-cell adhesion mechanism would maintain the tumor cells compactness, and thus would lead to a necrotic core, where cells in the center of the tumor are dead because of the lack of sufficient nutritionist. On the contrary, down regulation of the cell-to-cell adhesion leads to papillary tumor morphology where the tumor consists of branches. This shape is usually associated with metastasis [18].

Note that the process of the tumor metastasis is complex and not fully understood and goes beyond the scope of this project.

Another important factor that characterizes cancer is the ability of cancer cells to avoid detection by the immune system, which constantly surveys the body for abnormalities to eradicate. Naturally, the body fights tumor cells mainly with cytotoxic T lymphocytes, CTLs, and natural killer cells, NKs. Healthy cells are distinguished from tumor cells by antigens that cancer produces. Some tumor cells develop ways of altering or eliminating the antigen production, and also develop immunosuppressive properties, leading to the tumor escaping the immune surveillance. All of these alterations occur before the tumor is large enough for clinical detection [32].

NK cells and CTLs work in different ways. One important difference is that NK cells have the ability to kill only very few tumor cells, whereas CTLs can kill several during their lifetime [33]. For this reason, the model we developed is focused exclusively on CTLs. These are present throughout the body and in high concentrations in the lymph nodes. Created in the thymus, once they leave they are called "naive" CTLs, and are considered to be naive until exposed directly to antigens or altered via specific immune cells. This commonly occurs through antigen processing cells (APCs) that seek them out in the lymph nodes. They thus become activated and start expressing a special antigen-binding molecule on the surface: some of these activated cells turn into memory CTLs and divide, others become effector cells which attack the target. This is a complex process, see Fig. 2. The effector CTLs may kill the target either by cell-to-cell contact or by mechanisms mediated by cytokines. Given all this, in general CTLs have a special ability to recognize antigens produced by cellular alterations in tumor cells [34]. With adjuvant therapy, the immune system can be activated and enhanced and this is the principal scope of immunotherapy. Trials have been conducted involving early activation of the immune system leading to eradication of the cancer before it develops into dangerous and motile tumors, [20, 35, 36]. The purpose of this study is to investigate the effect of the immune systems response to various factors affecting tumor growth.

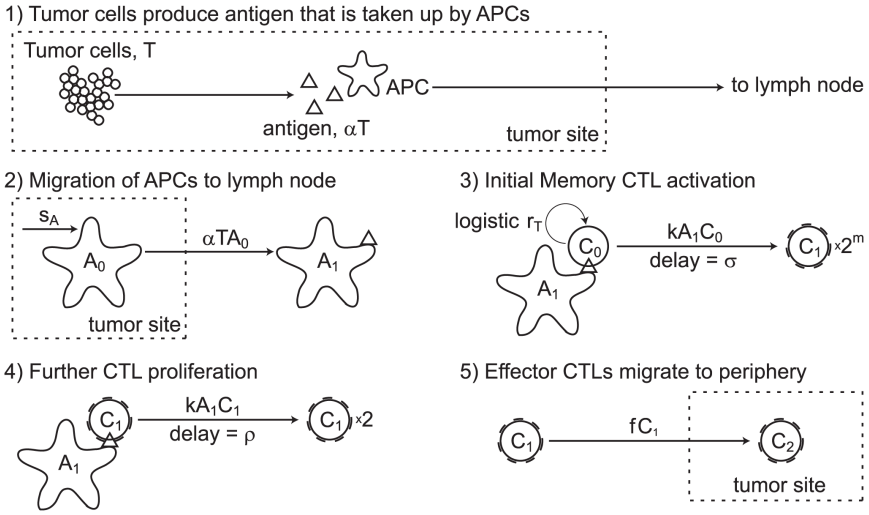

Figure 2: The CTL activation process, 1: as the tumor grows the tumor cells starts to produce antigens which get picked up by APCs, 2: the APSc mature and migrate to the lymph node, 3: in the lymph node the memory CTLs get activated by the mature APCs and enters the division program, 4: CTLs continues to divide, 5: effector CTLs migrate to the tumor site. Reprinted from Ref. [19].

1.3 Tumor growth trend

How a tumor grows is of great importance both for the understanding of tumor morphology and the fact that chemotherapy and radiotherapy is dependent upon it. Tumor growth is a complex mechanism that has been explained in different ways without reaching a unified consensus. Many tumor growth models are based on the assumption that tumors grow exponentially. Some models adopt an exponential growth model and some a combination of different laws. Bru et al. have recently proposed that the growth of the radius of a tumor is linear [37]. Drasdo et al. have suggested an exponential growth followed by a linear growth [38]. The same results are found by Mallet et al. for spherical tumors, but for papillary tumor morphology the growth is found to stay exponential without reaching linearity [10]. An extension on the exponential growth model is the Gompertzian growth model [39]. This is a special case of the generalized logistic function but it is not symmetric around its point of inflection. The Gompertz function has been used to explain many biological growth phenomenons [40], and since the 1960s it explains tumor growth to a good degree. Both in vivo and computational models have been proved to fit very well [41]. In this paper the tumor growth trend will be investigated.

1.4 Motivation and structure

The focus of this project is to investigate how the eradication of a tumor depends on the motility and adhesivity of the cancer cells. This project is built upon a previous ABM-DDE model in three dimensions by Kim et al., [19], simulating the interaction between tumor cells and the immune system. In that approach the tumor cells are simply stationary. The aim of this project is instead to add movement to cancer cells throughout the use of an effective physical potential, dependent upon the position of neighboring cells, so that each tumor cell's move is accepted or rejected via the use of the Metropolis approach. We further investigate time to eradication/ probability of eradication with respect to the movement of the tumor and cell-to-cell adhesion. Also, spatial distribution measurements for the tumor are used. These measures include radius of gyration, roughness and cluster distribution of the tumor cells, both for all tumor cells and only for the tumor cells with a variable number of neighbors. The effects of radius of gyration and roughness on the time to eradication of the tumor are studied. It turns out that a measurement of shape and density is necessary to quantify tumor responses appropriately.
In other words, well-defined observables help to understand, to some extent, what factors the eradication of a motile micro-tumor is dependent upon.

In Chapter 2, a succinct discussion of the mathematical and physical backgrounds relevant for the thesis is presented. In Chapter 3, results are shown and discussed with focus on parameter estimation and their variations. Finally, chapter 4 draws the conclusions for this study.

2 Models and methods

2.1 A previous model for static, solid tumors (Kim and Lee model)

Kim and Lee [19] have created a model that simulates the interaction between a growing tumor, the lymph node and CTLs after "priming" by a prophylactic cancer vaccine. This three-dimensional model is built upon both an agent based model (ABM) and delay differential equations (DDE). This particular combination was used to allow probabilistic treatments of tumor site and the dynamics of the lymph node. The study was focused on the CTL response to micro tumors that are too small for clinical detection and have yet not developed immunosuppression or immune evasive capabilities or the ability to migrate.

2.1.1 Model description

The ABM component of the model simulates the dynamics of the CTLs and tumor cells at the tumor site. The tumor site is a fixed space of radius R and outside this sphere the CTLs exist at a certain concentration, $C_2(t)$, determined by the DDE. To account for CTL movement outside the tumor site a CTL cloud of a height larger than the distance a CTL can move in a time-step is created. In the beginning of each time-step this cloud is filled with $C_2(t) \cdot V_{cloud}$ CTLs at random positions, chosen such that no overlapping with other agents occur.

The CTL movement is modeled by a three-dimensional Wiener process and in each time-step, Δt, each CTL takes a step $\overline{v}\Delta t$ in a random direction where each coordinate has normal distribution $\mathcal{N}(0, \sigma^2\Delta t)$, σ^2 is the variance in a CTL's speed and is related to the diffusion rate D by $\sigma^2 = 2D$. If the path of the CTL crosses any other cell, the agent goes as far as it can without overlapping and stops.

If a CTL at any point comes in contact with a tumor cell it can recruit another CTL with the probability $1/C_{recruit}$ on that site. If the recruitment is successful, a CTL will appear in a random direction next to the original CTL, and will only be included in the model if there is no overlap.

When in contact with a tumor cell, the CTL can potentially kill the tumor cell, with a probability given by $1-e^{-\Delta t/C_{kill}}$. If the tumor cell dies, the CTL begins to move again: it accelerates up to the maximum standard deviation, σ_{max}, with time dependent deviation given by $\sigma(t) = \sigma_{max} \cdot min(1, t/C_{acc})$, where C_{acc} is the average time it takes for a CTL to reach σ_{max}. At each time-step a CTL dies with the probability $1 - e^{-\Delta t/C_{death}}$, and one tumor cell will divide, in a similar manner to how CTLs recruit, with a probability of $1 - e^{-\Delta t/T_{div}}$. All dead components are removed from the system.

The dynamics of the lymph node is captured in a DDE system. As a tumor grows, so does the number of APCs with an initial concentration A_0. Once they become mature, with concentration A_1, they present tumor antigens. APCs migrate to the lymph node and cause memory CTLs, of initial concentration C_0, to enter a minimal division program. The CTLs that have completed the minimal division program become effector CTLs, with a concentration C_1, and continue to divide. These migrate to the periphery, at a concentration C_3, and this leads to a CTL response against the tumor site, see Fig. 2. According to Kim and Lee [19] this is captured by the following DDEs:

$$
\begin{cases}
A_0'(t) = & s_A d_0 A_0(t) - \alpha T(t) A_0(t) \\
A_1'(t) = & V_{ratio} \alpha T(t) A_0(t) - d_1 A_1(t) \\
C_0'(t) = & r_C \left(1 - \frac{C_0(t)}{K}\right) C_0 - \mu A_1(t) C_0(t) \\
C_1'(t) = & 2^m \mu A_1(t-\sigma) C_0(t-\sigma) - \mu A_1(t) C_1(t) + 2\mu A_1(t-\rho) C_1(t-\rho) + \\
& -\delta_1 C_1(t) - f C_1(t) \\
C_2'(t) = & \frac{f C_1(t)}{V_{ratio}} - \delta_1 C_2(t)
\end{cases}
\tag{1}
$$

The first line in Eq.(1) simulates the APCs waiting in the periphery of the lymph node. These are generated at a constant rate, s_A, and die at a proportional rate, d_0. The rate of APC stimulation is proportional to the tumor population, $T(t)$, with proportionality constant α related to the antigenicity of the tumor. If no stimulation occurs, the population stays at its equilibrium level s_A/d_0.

The second term simulates the maturation, antigen presentation and migration of the APCs. The first factor on the right hand side pertains to the rate at which the APCs enter the lymph node. To account for the different volumes of the tissue and the draining lymph node, the volume ratio, V_{ratio}, between them is used. The second factor accounts for the death of APCs.

The third expression relates to the memory CTLs in the lymph node. The population is increased with rate r_C until it reaches an equilibrium capacity K. The population dynamics follows a logistic growth model. The second term of the equation is the rate of stimulation by mature APCs and follows the mass action law where μ is the mass action coefficient.

The expression for $C_1'(t)$ simulates the effector CTLs that have ended the division process. The CTLs divide m times and the first factor is the rate of memory CTLs that enter the effector state, which is the same as the rate at which mature APCs stimulate the CTLs with an added time delay, σ. The increase in CTL population is 2^m. The second term is the rate at which CTLs become stimulated for further division. Then, the re-entry of a CTL into the system after the time of a cell division ρ is considered. Finally, the death rate δ_1 of CTLs that have completed the division program and the last term corresponding to the flow of CTLs out to the tissue at rate f, are included.

The last line pertains to the effector CTLs in the tissue via their flow out from the lymph node scaled by the volume difference V_{ratio} and their death.

These equations are translated into difference equations to enable their incorporation within the ABM. This process is based upon a number of assumptions: the variables in the DDEs are constant during small time-steps, Δt; the rates of state transitions across the time-steps are governed by Poisson process closely followed by mean field rates; the immune populations in the lymph node are constant. To take time delay into account, population values are included not only from the preceding difference equation time-step but also from the time-steps before that. The rewritten equations become:

$$
\begin{cases}
A_0^{n+1} = & s_A\Delta t + (1-p(d_0))A_0^n - p(\alpha T^n)(1-p(d_0))A_0^n \\
A_1^{n+1} = & V_{ratio}p(\alpha T^n)(1-p(d_0))A_0^n + (1-p(d_1))A_1^n \\
C_0^{n+1} = & (1+p(r_C(1-\frac{C_0^n}{K})))C_0^n - p(\mu A_1^n)C_0^n \\
C_1^{n+1} = & 2^m p(\mu A_1^{n-a})C_0(n-a) + (1-p(\delta_1))C_1^n - p(\mu A_1^n)(1-p(\delta_1))C_1^n \\
 & +2p(\mu A_1^{n-b})(1-p(\delta_1))C_1^{n-b} - p(f)(1-p(\delta_1))(1-p(\mu A_1^n))C_1^n \\
C_2^{n+1} = & \frac{1}{V_{ratio}}p(f)(1-p(\delta_1))(1-p(\mu A_1^n))C_1^n + (1-p(\delta_1))C_2(t)
\end{cases}
\tag{2}
$$

where $a = \sigma/\Delta t$, $b = \rho/\Delta t$ and $p(y) = 1 - e^{-y\Delta t}$ is the transition rate modeled by deterministic factors.

The different terms in Eq.(2) have the same meaning as in Eq.(1). The terms $(1 - p(d_x))$ represent the probability of the survival of the cell to the next step and hence $(1 - p(d_x))Y_x^n$ is the concentration, with d_x and Y_x^n being system variables. Note that $p(\alpha)$, $p(\mu)$ and $p(f)$, together with the concentration, are probabilities and replace the transition rates in Eq.(1) taking the probabilistic nature of the ABM into account. All this allows the equations to be updated discretely and simultaneously [19].

In essence, the model by Kim and Lee simulates the interaction between a growing tumor and the body's defense against it where the immune system is trying to inhibit the tumor from growing. This interaction is captured by using a ABM-DDE model.

2.1.2 Results

The findings of the study by Kim et al. [19] show that, with no restrictions on the time scale of the simulation, all tumors will be eradicated. This is predominantly due to the fact that the CTL recruitment time is always larger than the tumor cell division time. The time to eradication and maximum tumor size are important since it is believed that the lower these are the less likely tumor metastasis and its migration are. These properties depend mainly on the tumor antigenicity, the CTL recruitment rate, the memory CTL population pool and the tumor cell division time. Since the antigenic signal is weak, a faster growing tumor becomes detected faster, and therefore eliminated faster than a slower growing tumor. However, these rapid growing tumors reach larger sizes and therefore become more likely to reach a migrating size. As such, according to this framework, the fastest and slowest growing tumors are the most problematic and potentially dangerous ones.

Interestingly, the tumor cell number decline is also found to follow a cubic, as opposed to an exponential, decline to extinction. This leads to a deterministic, certain extinction, where the tumor cell count reaches zero in finite time.

Overall, this model suggests that vaccinations against tumor cells which create memory CTLs could prevent tumors from reaching an average size of approximately 1000 cells and that an effective vaccine could be a feasible strategy against cancers. One of the main insights of this model is that, generally, between 3% and 5% of the total T-cells in the lymph node need to be primed to have a successful response against tumors of this kind (i.e solid and small).

2.2 A novel approach for motile cancer cells

To expand on the previous model by Kim and Lee tumor cell mobility is added via a physical force. The tumor cells are assumed to interact with each other with a repulsive and adhesive force creating a potential. A number of shape measurements are also added to investigate what parameters the outcome of the simulation is dependent on.

To simulate tumor mobility a combination of the following parts are used.

2.2.1 Description of tumor mobility

How and why cells move is still widely discussed. Some of the quantitative models that try to describe cell motility include Brownian motion, persistent random walk and fractional Klein-Kramers processes, see [19, 38, 42]. In our approach chemotaxis is not taken into account and the individually moving tumor cells are therefore assumed to behave in a random walk like fashion, in line with in vivo experiments [43]. Note that chemotaxis is the phenomenon occurring when a cell (or multi-cellular organism) orientates itself along a chemotactical gradient, favoring higher gradients, to move in a certain direction [44]. We use a Wiener process similar to that for a CTL, where the step is randomly chosen, in each direction, from a normal distribution $\mathcal{N}(0, \sigma^2\Delta t)$, with zero median such that $\sigma^2 = 2D$. The step is either accepted or rejected depending upon the change of the total energy of the system, using the Metropolis algorithm, [45]. This method has previously been used in studies on cancer growth and movement, e.g. by Drasdo et al., [38]. A step will be accepted with probability

$$p \propto min\left(1, e^{-(\sum_{i<j}(V_{ij}(t+\Delta t)-V_{ij}(t))/F_T}\right) \tag{3}$$

where F_T is a reference energy analog to k_BT, where k_B is the Boltzmann constant and T is the temperature of the system.

The step will always be accepted if it leads to an energy decrease. If it instead leads to an energy increase, it will be accepted with an exponential probability distribution, depending on F_T. The use of a canonical distribution and Maxwell-Boltzmann statistics is a common approximation in cancer growth [46]. Typical ranges for the reference energy F_T are given by F_T $10^{-17} - 10^{-15}J$ [47, 48]. Metropolis algorithm helps minimize the energy on a global level for the system [49].

2.2.2 Interactions for tumor cells

Cells that are in close proximity to each other interact. When they become sufficiently close they can create adhesive bonds, however, when they become too close they experience a repulsive force, which prevents them to overlap [50]. There are several methods of modeling this interaction (see Refs. [14, 51]) but studies have shown that, qualitatively, similar trends emerge in the overall behavior of the system [18, 52]. Tumor cells in this numerical experiment are assumed to keep their spherical shape and constant radius during interaction, this is in accordance with several previous models (see Refs. [38, 46]). We thus choose to use a center of mass to govern the interactions and not consider the use of local sites on the cells (sometimes called "sticky" sites) through which adhesion is mediated.

To model adhesion a soft cosine force is used. This is similar to a square well potential and computationally convenient to use [14]:

$$\mathbf{F}_{ij}^{CCA} = \begin{cases} -\frac{\epsilon_{CCA}\pi}{r_{cut}^{CCA}} \cos\left(\frac{\pi \mathbf{r}_{ij}}{r_{cut}^{CCA}}\right) & r_{ij} \leq 2r_{cut}^{CCA}, \\ 0 & \text{otherwise} \end{cases} \tag{4}$$

The potential is thus:

$$\mathrm{V}_{ij}^{CCA} = \begin{cases} -\epsilon_{CCA} \sin\left(\frac{\pi \mathbf{r}_{ij}}{r_{cut}^{CCA}}\right) & r_{ij} \leq 2r_{cut}^{CCA}, \\ 0 & \text{otherwise} \end{cases} \tag{5}$$

where r_{cut}^{CCA} is the cut-off radius for adhesion, r_{ij} is the distance between cell i and j and ϵ_{CCA} is the force coefficient.
The repulsive force is modeled as a cubic function, dependent upon the distance between the two cells. When the two cells overlap with more than a certain compressibility constant, α_c, they are hit by an infinite potential wall. This can be described by the force:

$$\mathbf{F}_{ij}^{CCR} = \begin{cases} \frac{8\epsilon_{CCR}}{\delta^2}(2r - \mathbf{r}_{ij})^3 & 2r - \delta \leq r_{ij} < 2r, \\ \infty & r_{ij} < 2r - \delta, \\ 0 & \text{otherwise} \end{cases} \tag{6}$$

which gives the potential:

$$\mathrm{V}_{ij}^{CCR} = \begin{cases} \frac{4\epsilon_{CCR}}{\delta^2}(2r - \mathbf{r}_{ij})^4 & 2r - \delta \leq r_{ij} < 2r, \\ \infty & r_{ij} < 2r - \delta, \\ 0 & \text{otherwise} \end{cases} \tag{7}$$

where r is the cell radius, r_{ij} is the distance between cell i and j, ϵ_{CCR} is the force coefficient and δ the structural softness depending on the compressibility, α_c, $\delta = 2\alpha_c r$, [12].
The use of a repulsive term takes into account the obvious fact that cells cannot penetrate each other, but the model allows cells to overlap for finite, small portions, thus encapsulating the ability of each cell to slightly deform when adhering to a neighbor.

2.2.3 Algorithm

The combination of the old tumor-immune system interaction together with the added tumor mobility leads to a new simulation consisting of the following steps:
0. Initialize parameters, tumor and ABM-DDE model
1. Determine CTL concentration in CTL cloud
2. Update CTL actions
    case 1: CTL is in contact with a tumor cell
        Determine whether the CTL will kill the tumor cell
        Determine whether the CTL will recruit another CTL to the tumor site
    case 2: CTL is not in contact with a tumor cell
        Perform random walk for CTL
3. Update tumor cell actions
        Determine whether tumor cell will divide
        Else perform random walk on tumor cell and determine forces acting before and after the move, accept using Metropolis algorithm

4. Calculate new positions and update ABM-DDE model accordingly

Repetition of step 1-4 until end of simulation is performed for each of the results shortly discussed.

2.3 Observables and shape measures

To understand the dynamics of small, solid tumor and how motility affects their development several shape measures and observables are introduced. Previous studies have shown that the malignancy of a tumor can be assessed to some extent using its shape. It is therefore important to understand the dependent factors that affect its morphology [15].

The radius of gyration is a measure of the distance and spatial distribution of cells from the center of mass and can be calculated by:

$$R_g = \left(N_c^{-1} \sum_{i=1}^{N_c} (\mathbf{r}_i - \mathbf{r}_{cm})^2 \right)^{1/2} \tag{8}$$

where N_c is the total number of cells, $\mathbf{r}_i$ the location of cell i and $\mathbf{r}_{cm}$ the location of the center of mass of the tumor [14].
The radius of gyration can also be generalized to define the gyration tensor

$$\mathbf{R}_g^2 = \langle N_c^{-1} \sum_{i=1}^{N_c} (\mathbf{r}_i - \mathbf{r}_{cm})(\mathbf{r}_i - \mathbf{r}_{cm}) \rangle, \tag{9}$$

which gives a thorough description of the spatial properties of the cancer mass.
The eigenvalues of the tensor of gyration will have the following property:

$$0 \leq \frac{l_3}{l_1} \leq \frac{l_2}{l_1} \leq 1$$

As the shape gets more and more spherical these ratios gets closer to one [53]. These can be used to evaluate the acylindricity, b, asphericity, c, and the relative shape anisotropy, κ, by

$$b = l_1 - 0.5(l_2 + l_3) \tag{10}$$

$$c = l_2 - l_3 \tag{11}$$

$$\kappa^2 = \frac{b^2 + (3/4)c^2}{R_g^4} \tag{12}$$

The asphericity measures the displacement from symmetry in three dimensions. It is zero only when $l_1 = l_2 = l_3$ and the object is completely symmetric around the three coordinate axes. This occurs when it is spherically symmetric and when it is in the shape of a tetrahedron or any object with a higher symmetry. The acylindricity works in a similar way but only takes the two smallest eigenvalues into account and is therefore a measurement of how cylindrical the object is. When the anisotropy is zero the object has a spherical symmetry and when it is one it is linear. The relative shape anisotropy is

bounded between these two values [54].
Another dynamical property is the roughness of the tumor. Studies have shown that the roughness can be use as an indicator of the malignancy of the tumor, [15].

$$R_{rough} = N_{bin}^{-1} \sum_{i=1}^{N_{bin}} \left((d_i - \langle d \rangle^2) \right)^{1/2}, \tag{13}$$

with

$$\langle d \rangle = N_{bin}^{-1} \sum_{i=1}^{N_{bin}} d_i,$$

where N_{bin} is the number of equally sized bins the sphere is divided into and d_i the distance to the farthest cell in bin i.
The roughness can vary greatly depending on many factors, however, it is found to be time dependent and have a value between 10 μm and 75 μm for an early stage tumor in numerical experiments by Jeon et al. [14].

3 Results and discussion

3.1 Typical outcomes of model simulations

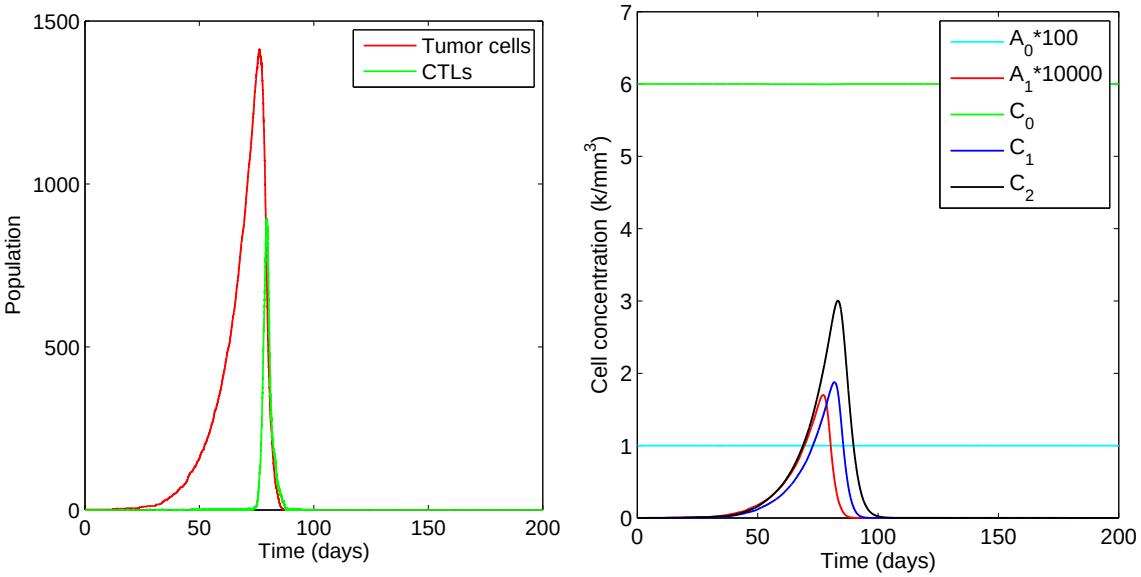

(a) (b)

Figure 3: Eradication of a motile tumor with $\sigma_{\text{Tumor}} = 0.2$ μm min^{-1}, $\epsilon_{CCA} = 1.5 \cdot 10^{-16}$ m^2 kg s^{-2} for (a) the evolution in time of the ABM-DDE model with the CTL and tumor cell populations. (b) the corresponding variables in the DDE, where the parameters are governing the APC-CTL process.

To understand the ABM-DDE model and also to observe the tumor-CTL interactions an example simulation can be viewed in Figs. 3-4. It should be noted that due to the high stochasticity of the model different outcomes depending on different tumor evolutions are possible. Fig. 3(a) shows the evolution in time of the ABM-DDE model with the CTL and tumor cell populations, whereas Fig. 3(b) illustrates the corresponding variables in the DDE, where the parameters governing the APC and CTL populations are followed. In this simulation the tumor cells are motile. When the tumor cell concentration increases, more and more APCs mature and gives rise to a CTL response at the tumor site, commencing at day 70, as discussed in section 2.1 above. Since the rate of CTL recruitment is higher than the rate of tumor divisions and the CTLs can kill more than one tumor cell each, the tumor population begins to decrease at day 76 and tumor population 1410. Finally, the tumor is completely eradicated at day 87. Since the variables in the DDE all are dependent on the tumor cell population the APC-CTL process is delayed, compared to the tumor growth. The concentration of mature, antigen presenting and migrating APCs starts to increase and the CTL population follows closely to rise faster and give rise to a high and quick growing CTL response at the tumor site. Since the rate of maturation and stimulation of APCs and CTLs is very low the population of immature APCs and memory CTLs remains almost constant. Corresponding snapshots can be found in Fig. 4 where the interaction between the CTLs and the tumor cells on the tumor site are illustrated. Fig. 4(a) is taken on day 70 when the tumor has started growing and is still not "noticed" by the CTLs, one CTL is on the tumor site but the tumor goes "unnoticed". By day 77 the CTL attack has started, Fig. 4(b), and by day 79 the CTLs have overpowered the

tumor and its size started decreasing, Fig. 4(c). The last figure, Fig. 4(d), pertains the tumor site when the tumor is completely eradicated and only a couple CTLs are left at the tumor site, these will migrate away or die.

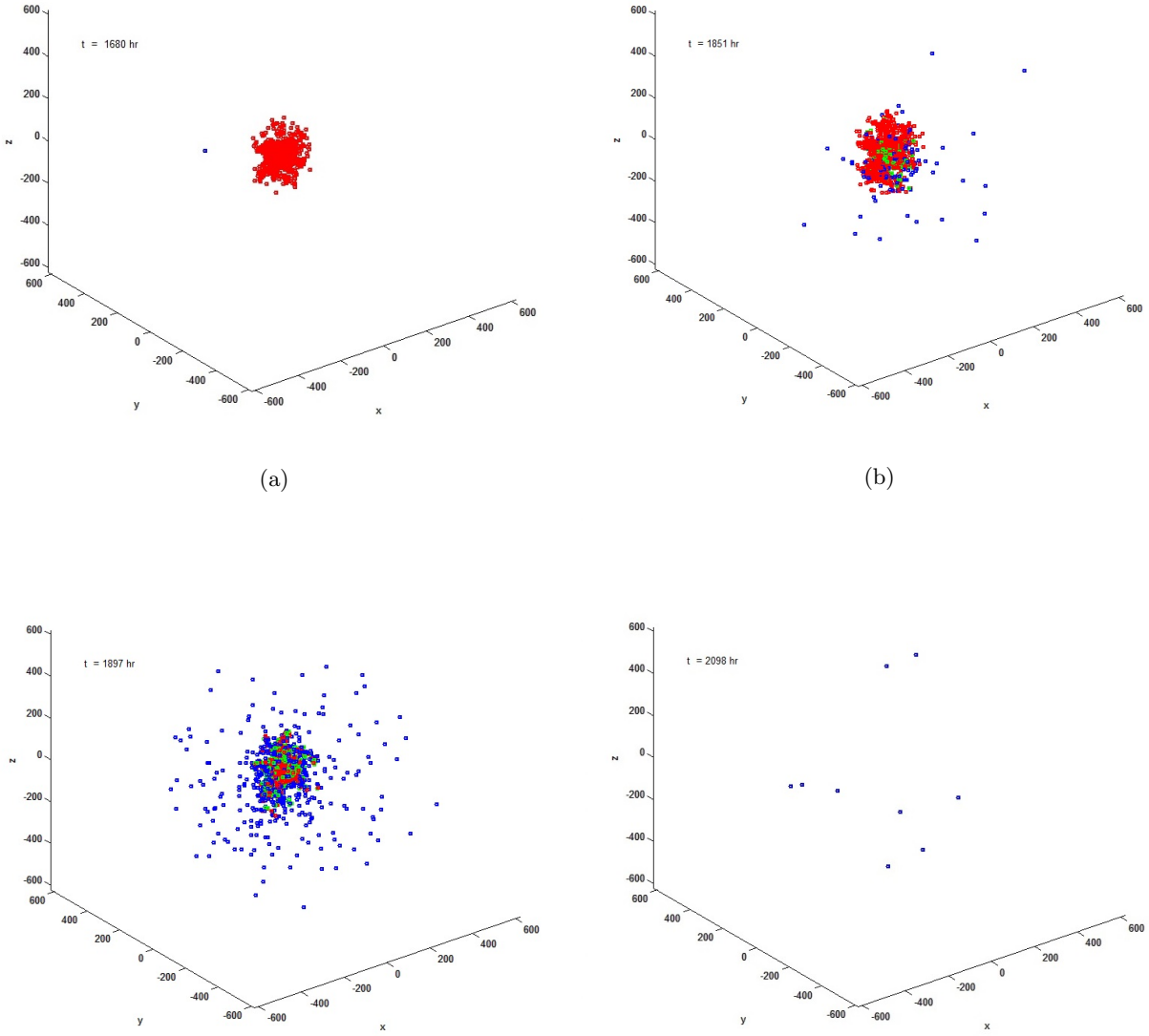

(a) (b)

(c) (d)

Figure 4: Snapshots of a motile tumor with $\sigma_{\text{Tumor}} = 0.2\ \mu\text{m min}^{-1}, \epsilon_{CCA} = 1.5 \cdot 10^{-16}\ \text{m}^2\ \text{kg s}^{-2}$, red dots represent the tumor cells, blue dots represent the CTLs and green dots represents the killed tumor cells that are not yet processed by the body, for (a) day 70 when the tumor has started growing and is still "unnoticed" by the CTLs, (b) day 77 when the CTL attack has started, (c) day 79 where the CTLs have overpowered the tumor and its size started decreasing and (d) day 87 when the tumor is completely extinct and some CTLs are left at the tumor site. They will migrate away or die very soon. Note that the times of the snapshots are in hours.

A simulation for a moving tumor with a different outcome can be seen in Fig. 5, where the tumor goes through several relapse cycles and eventually becomes too large for the simulation to continue. In this and following results, we choose to stop computations when the tumor growth period reaches a time of 200 days or, in case of very large tumors, when we ran out of computational power. Each time the CTL response attacks the tumor, a small number of tumor cells avoid eradication after the CTL response. Since they are low in number, they will not produce sufficient antigens for the CTL response to remain active, and as the CTL response is reduced, the tumor begins dividing and is allowed to relapse. These findings are in line with results found by Mallet et al. [9]. Note that the velocity is considerably higher in this simulation than in the previous, illustrated in Figs. 3-4.

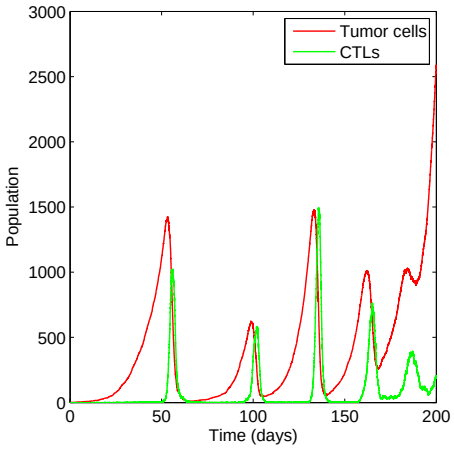

(a)

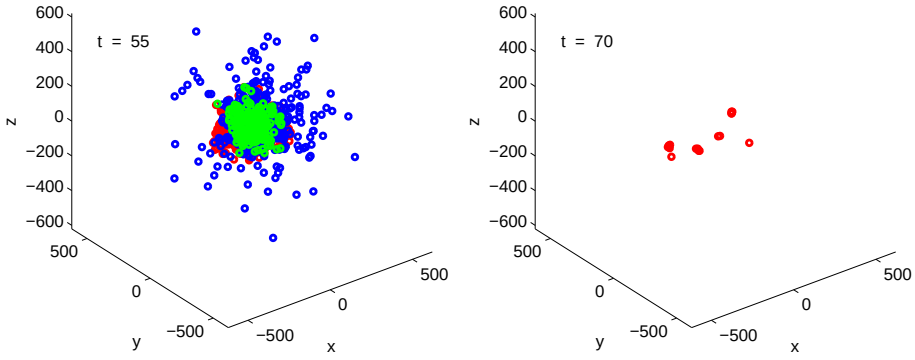

(b) (c)

Figure 5: Relapse of a motile tumor with $\sigma_{tumor} = 0.5\mu\text{m min}^{-1}, \epsilon_{CCA} = 1.5 \cdot 10^{-16}$ m^2 kg s^{-2} for, (a) the evolution of the population, (b) snapshot just before the first CTL attack, (c) snapshot just after the first CTL attack, where pockets of tumor cells survive and lead to a relapse. Red dots represent the tumor cells, blue dots represent the CTLs and green dots represent the killed tumor cells that are not yet processed by the body. Time is in days.

3.2 Tumor velocity dependence

The outcome from the simulations with different velocities in the previous section varied greatly. Let us now consider motile tumors in detail. To investigate the influence of tumor velocity on the outcome of immunotherapies, the standard deviation of the velocity for the tumor was varied. Simulations were performed for two different tumor velocity standard deviations, $\sigma_{tumor} = 0.15$ μm min^{-1} and $\sigma_{tumor} = 0.5$ μm min^{-1}. This is in agreement with typical speeds for biological cells, as explained in Ref. [55]. In Figs. 6-7 simulations where the CTLs are successful in eradicating the tumor ($\sigma_{tumor} = 0.15$ μm min^{-1}) and unsuccessful ($\sigma_{tumor} = 0.5$ μm min^{-1}) are compared.

Firstly, it can be observed that they look similar up until day 65. After this, the simulation with lower tumor velocity is successful in eradicating the tumor whereas the simulation with the higher is not. The latter instead reaches a low, non-zero tumor population but relapses and increases. It is also interesting to note that after each relapse the local minima in tumor population become larger and the CTLs leave more and more cells to relapse. At day 120 the CTL population drops, leaving a tumor of about 1000 cells, and this is followed by an exponential increase in tumor population. To investigate the distribution of singlets, doublets, etc. as time progresses, it is useful to look at Fig. 7. We keep track of the distribution of cellular clusters according to number of neighbors each tumor cell has, and plot the percentage of cells belonging to the different cluster. The percentage of cells in different sized clusters follow each other closely for the lower average velocity, leading to the singlets being most common, followed by the doublets, etc. For the higher average velocity the singlets dominate the tumor distribution from start, this behavior grows stronger with each relapse. The behavior of the singlets alone is interesting to study. In Fig. 7(b) the percentage of singlets is much higher than in simulation 7(a). This means that more single cells are present, which leads to a decrease in the antigen production per volume and the stochastic recognition by the CTLs. Consequently, there is a decrease in CTL population up to their complete depletion, and the tumor can successfully survive. This behavior is later repeated, causing a higher ratio of single cells to total cell count, in a sort of feedback mechanism that weakens the CTL response.

In Fig. 8, snapshots can be observed for the high velocity standard deviation simulation for the early stages of the first attack and before the second. It is apparent that a small number of cells have survived at different locations and then started to divide again leading to a considerably less dense tumor.

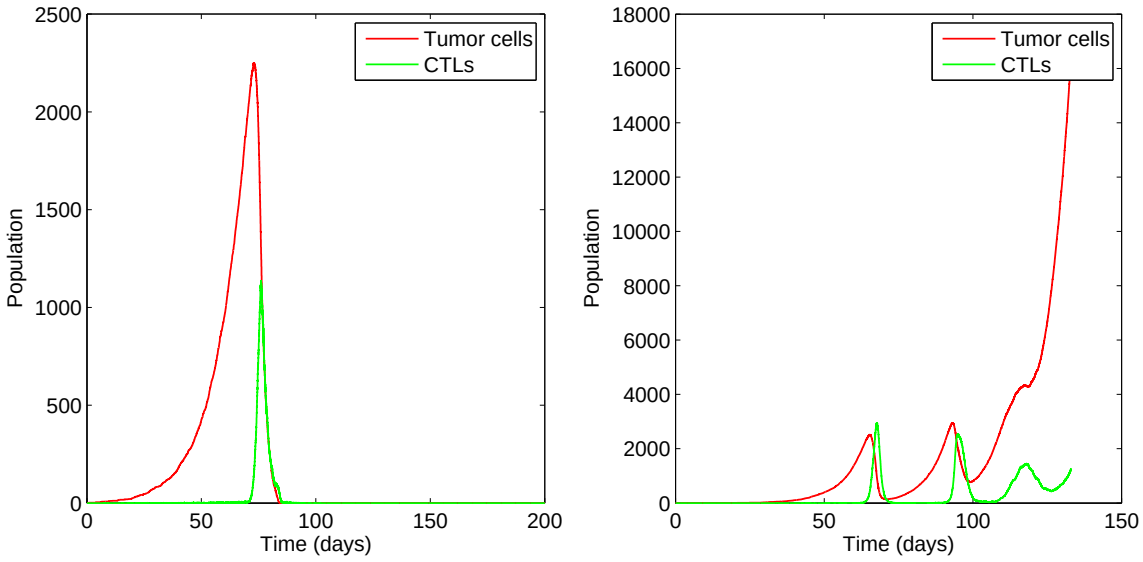

(a) (b)

Figure 6: Evolution of the population for a motile tumor with (a) $\sigma_{\text{Tumor}} = 0.15$ μm min^{-1}, $\epsilon_{CCA} = 1.5 \cdot 10^{-16}$ m^2 kg s^{-2} for eradication with success and (b) $\sigma_{\text{Tumor}} = 0.5$ μm min^{-1}, $\epsilon_{CCA} = 1.5 \cdot 10^{-16}$ m^2 kg s^{-2} for relapse.

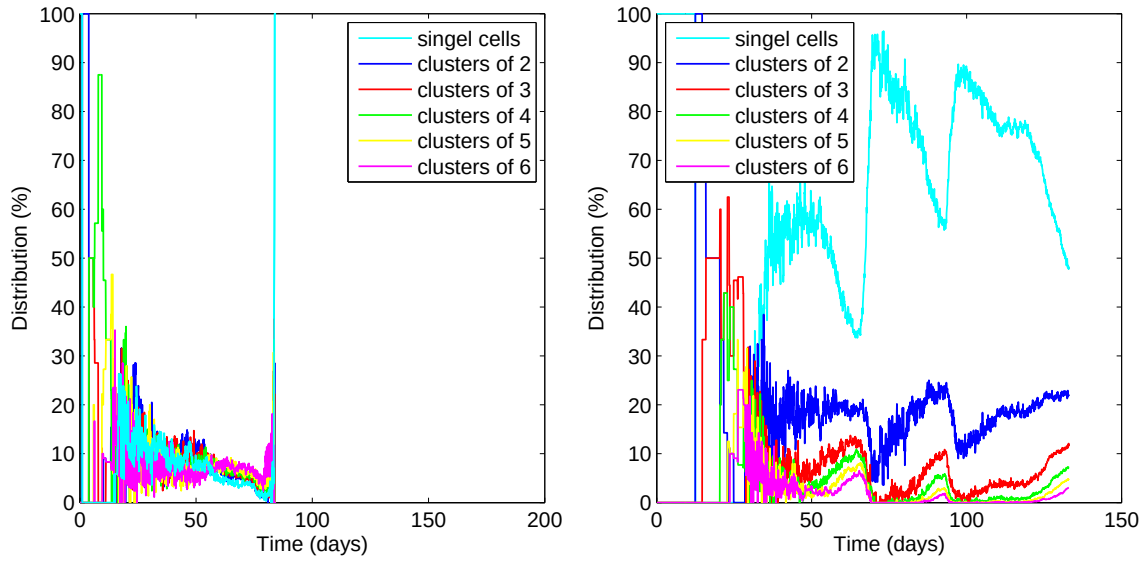

(a) (b)

Figure 7: Evolution of the distribution of cells for a motile tumor with (a) $\sigma_{\text{Tumor}} = 0.15\mu$m min^{-1}, $\epsilon_{CCA} = 1.5 \cdot 10^{-16}$ m^2 kg s^{-2} for eradication with success and (b) $\sigma_{\text{Tumor}} = 0.5\mu$m min^{-1}, $\epsilon_{CCA} = 1.5 \cdot 10^{-16}$ m^2 kg s^{-2} for relapse.

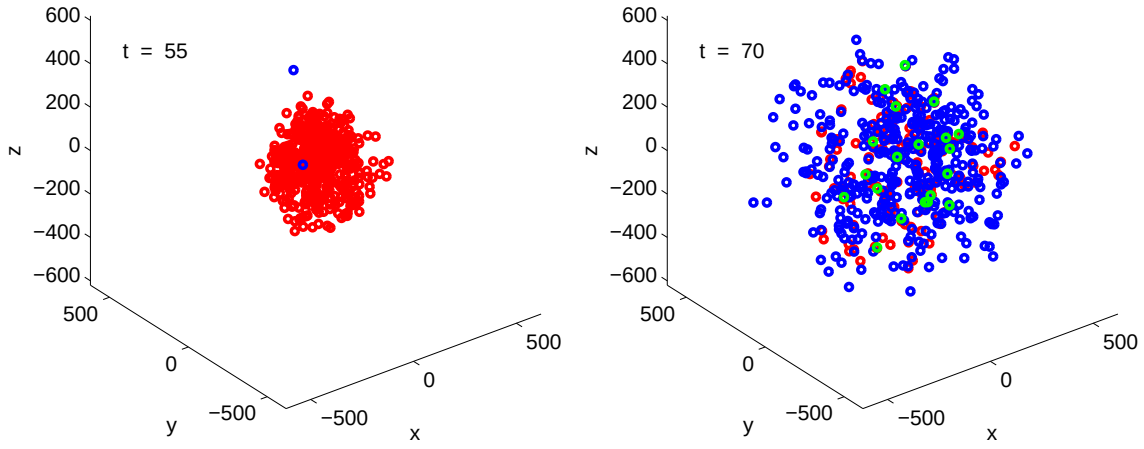

(a) (b)

Figure 8: Snapshot of a motile tumor for a non successful eradication with $\sigma_{\text{Tumor}} = 0.5\mu\text{m min}^{-1}, \epsilon_{CCA} = 1.5 \cdot 10^{-16}$ m^2 kg s^{-2}, red dots represent the tumor cells, blue dots represent the CTLs and green dots represent the killed tumor cells that are not yet processed by the body, (a) at the beginning of the first attack, (b) just after the first attack. Some cells survive the first attack and have now undergone division, with the result of making the tumor more diluted. Time is in days.

Interestingly, we found that results indicate that tumor relapse may occur also for tumors with low velocities, as seen in Fig. 9. This is a simulation with the same parameters as those in Figs. 6-7(a). Due to the probabilistic nature of the model, the cancer evolves differently and the outcome can be completely unpredictable. In this case, only one cell (see Fig. 9(b)-(c)) remains after the attack. This singlet causes the tumor to relapse and be eradicated after a second attack. This oscillatory behavior is well-known, and has been experimentally observed to some degree in chronic deceases such as leukemia [56, 57].

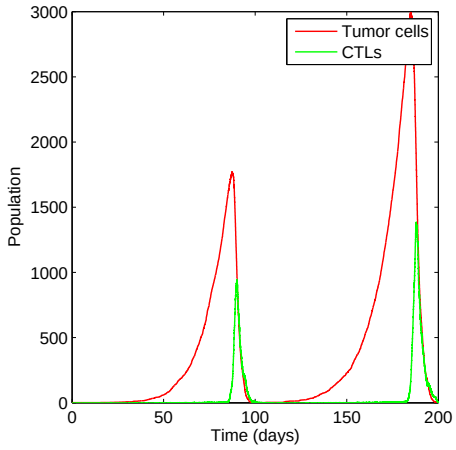

(a)

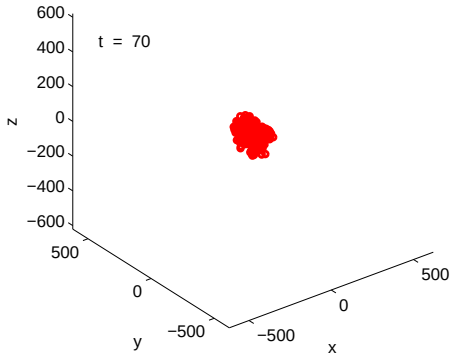

(b)

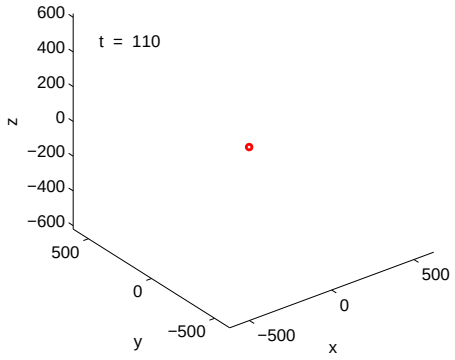

(c)

Figure 9: A motile tumor that relapses before eradication with $\sigma_{\text{Tumor}} = 0.15$ μm min^{-1}, $\epsilon_{CCA} = 1.5 \cdot 10^{-16}$ m^2 kg s^{-2} ;(a) the evolution of the population, (b) snapshot just before the first CTL attack, (c) snapshot just after the first CTL attack. Only one tumor cell survives and leads to relapse. Red dots represent the tumor cells, blue dots represent the CTLs and green dots represent the killed tumor cells that are not yet processed by the body. Time is in days.

A statistical analysis can be performed to investigate the different results yielded from simulations, comparing outcomes for lower and higher velocities. Ten simulations are run for each standard deviation between 0 μm min^{-1} and 0.5 μm min^{-1}, at 0.05 μm min^{-1} increments.

There appears to be a defined tumor standard deviation threshold, at approximately $\sigma_{\text{Tumor}} = 0.3$ μm min^{-1}, where tumors with a lower velocity standard deviation are eradicated and tumors with higher velocity standard deviation escaped (Fig. 10). After the threshold all the tumors escape. However, before the threshold the outcome is less certain and variability exists. The general trend is that the number of relapses and tumor escapes increases as the tumor velocity increases.

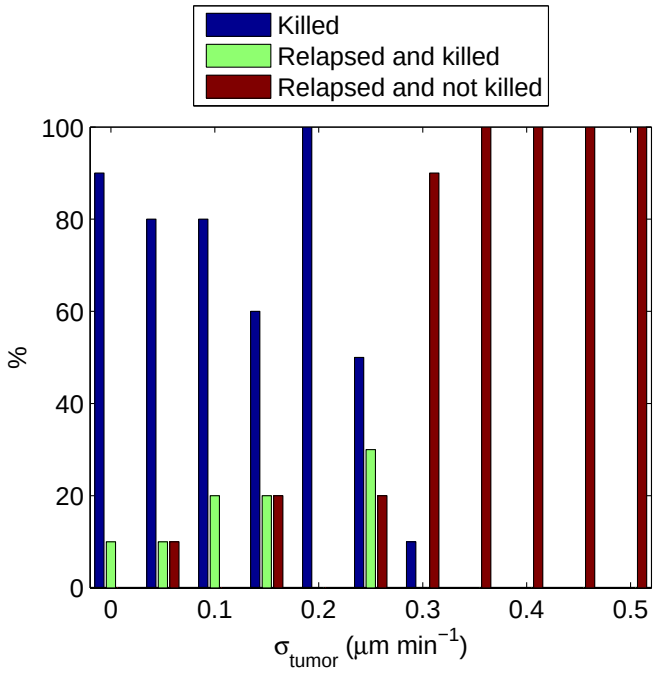

Figure 10: Histogram displaying the occurrence of different outcomes as a function of tumor velocity standard deviation. Note how all 10 runs at $\sigma_{\text{Tumor}} = 0.2$ μm min^{-1} led to eradication.

Further analysis is carried out to understand the influence of the tumor velocity standard deviation. There is a clear difference observed between the density for the different tumor velocities, with higher velocities leading to lower densities (see Fig. 11). The evolution of the density over time is similar for the different velocities: it is very high in the early stages when a tumor consists of very few cells, in some cases one cell. The density then decreases and stabilizes up to the start of the CTL response, when it suddenly becomes irregular before approaching zero.

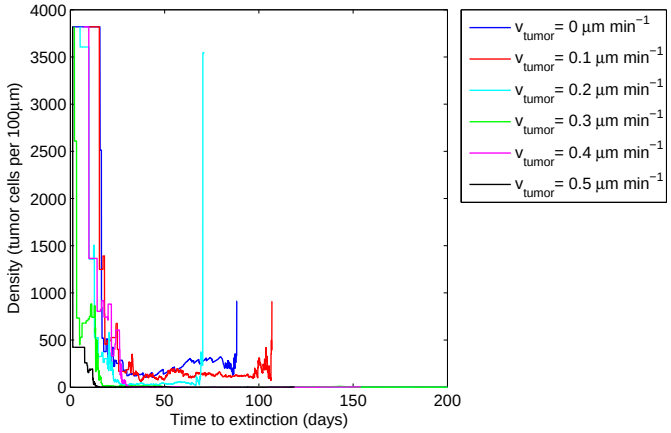

Figure 11: The density as a function of time for different velocities. Blue, red and yellow are eradicated.

This can be complemented by an analysis of the roughness and the radius of gyration of the tumor, as illustrated in Figs. 12-13. Increased velocity standard deviation is associated

with increased radius of gyration and roughness. At the same tumor cell number, tumors with higher velocities have a rougher, more spread out shape, which subsequently lead to a lower density. Each time the tumor relapses after a CTL attack the roughness and radius of gyration increases. This is clearly observable for tumors with standard deviation of 0.3μm min^{-1}, where relapse occurs less often and the roughness and radius of gyration become approximately constant between CTL attacks.

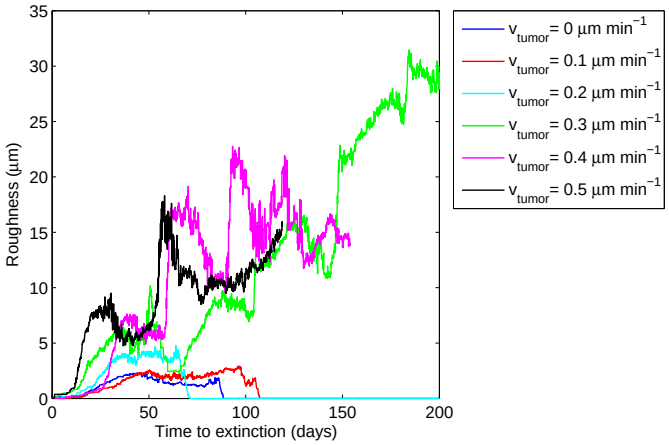

Figure 12: The roughness when all tumor cells are included as a function of time for different velocities. The magenta and black lines stops since these simulations were terminated due to reach of maximum computational time.

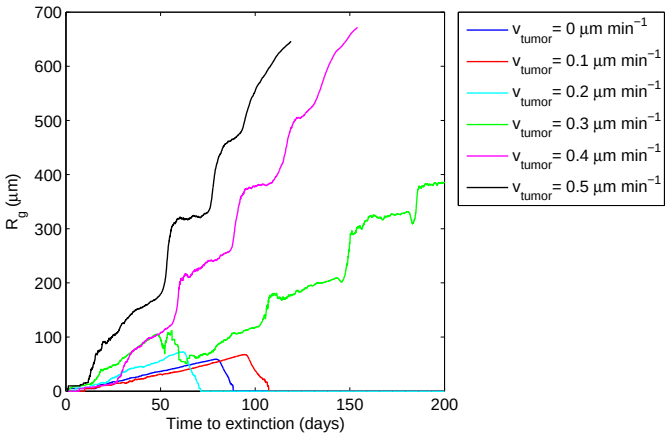

Figure 13: The radius of gyration when all tumor cells are included as a function of time for different velocities. The magenta and black lines stops since these simulations were terminated due to reach of maximum computational time.

The relationship between the relative proportion of single cells at different velocity standard deviations is plotted in Fig. 14. There is a clearly different behavior for low and high tumor velocities. After reaching a tumor number of approximately 10 cells the single cell distribution peaks for all the different tumor velocities. However, the lower ones only ever reach a very low distribution, and are almost stable after that. A slightly higher tumor velocity leads to a higher initial peak, followed by a linear decrease. Just before eradication the single cell distribution peaks before going down to zero. Relapsing tumors have a similar behavior but the top of the initial peak lasts longer and after each CTL attack

another peak occurs and the pattern is repeated with a generally higher distribution. The higher the single cell ratio, the more difficult for the CTLs to detect the tumor and less likely is a successful eradication is.
By determining the ratio of single cells and the behavior over time, an estimation of the probability of eradication can be obtained.

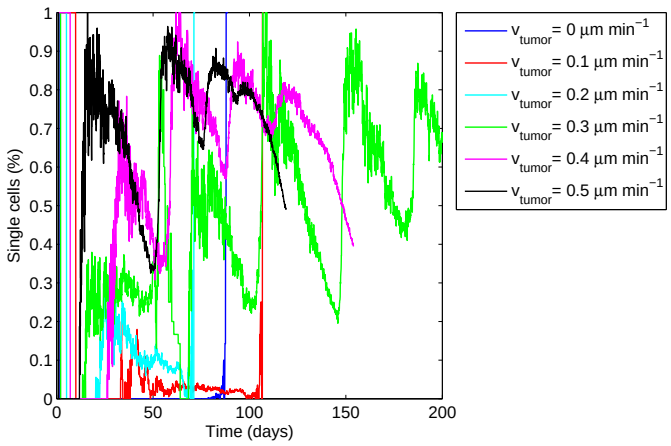

Figure 14: The distribution of single cells as a function of time for different velocities. The magenta and black lines stops since these simulations were terminated due to reach of maximum computational time.

3.3 Tumor velocity and shape dependence on immunotherapy outcome

It is important to discuss the predictive capabilities of this model. Is it possible to obtain indications about the likelihood of one outcome with respect to another?

First of all, to determine what parameters influence behaviors of therapies, the tumor is now permitted to grow to tumor cell number 3000 before the CTL response is allowed to start. This results in the dependence of the highly stochastic behavior on tumor growth speed (in the early stages of the simulation) to be "smoothed out" and allows a more consistent determination of time of eradication or escape. It also enables the measurement of the shapes when tumors are of the same size and when the shape only depends on the tumor velocity standard deviation.

It turns out that there is a correlation between the tumor velocity standard deviation and the different shape measurements, as explained by Fig. 15. The density appears to have an inverse, non linear dependence on the tumor standard deviation with higher variability for lower σ_{tumor}, see Fig. 15(a), whereas the roughness appears to have a linear relationship with the tumor velocity standard deviation with high variability for high σ_{tumor}, see Fig. 15(b). The radius of gyration appears to have a minimum at $\sigma_{tumor} = 0.05$ μm min^{-1} and then increase linearly. The radius of gyration has also the highest variability for high velocity standard deviations. Moreover, the growth speed seems to increase with the average tumor speed but it should be noted that there are great variability in the results, see Fig. 15(d). A higher standard deviation indicates a less dense, but larger and rougher tumor. This creates a better environment for the tumor to divide and grow.

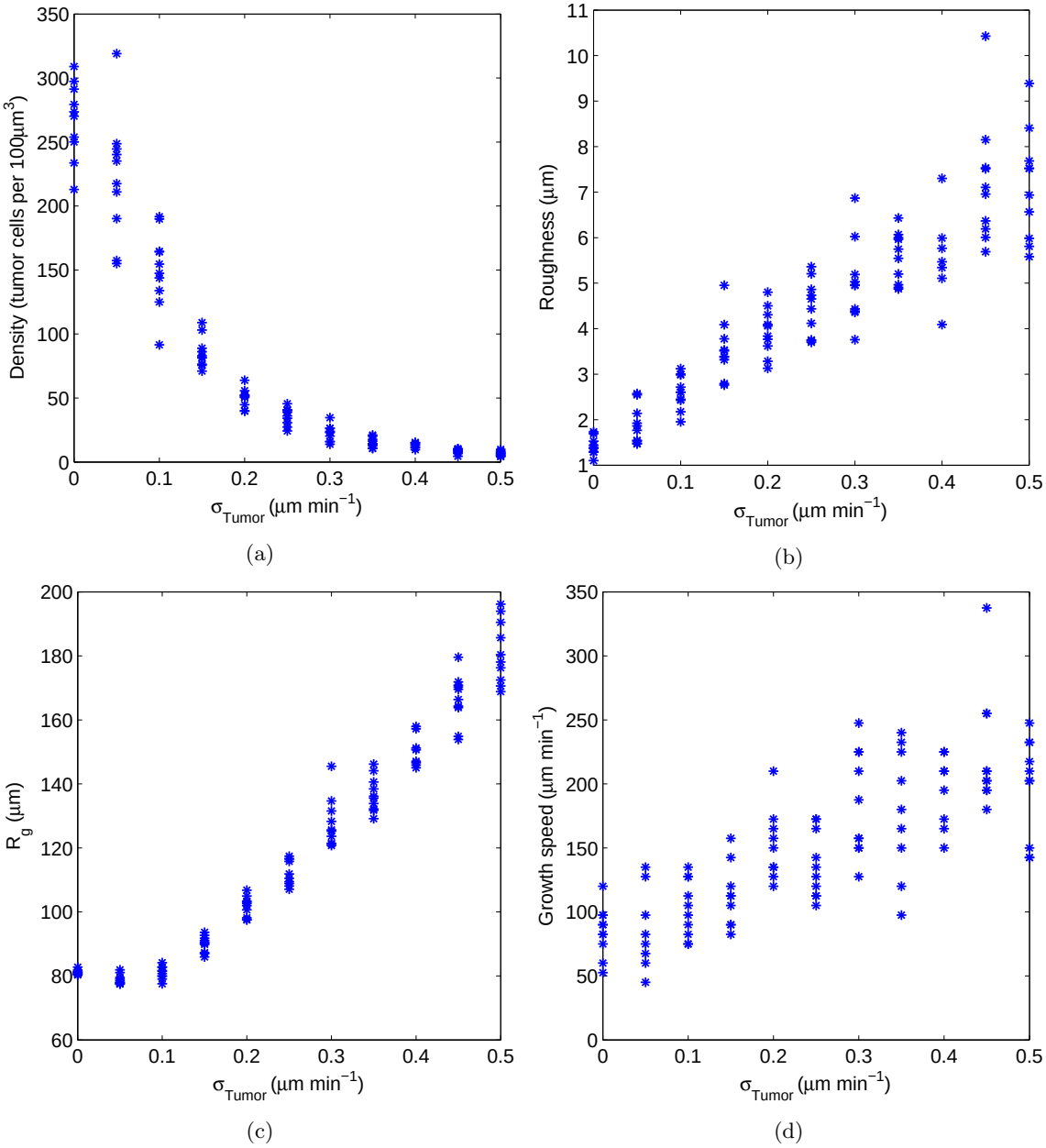

Figure 15: The effect of the tumor velocity standard deviation for a CTL response started at tumor size 3000 on (a) density, (b) roughness, (c) radius of gyration and (d) tumor growth speed. All measurements taken at size 3000 before CTL response.

The dependence of the tumor velocity standard deviation upon the gyration tensor properties is not as strong. There is a slight increase in the acylindricity and asphericity and decrease in the anisotropy as the tumor velocity standard deviation becomes higher, see Fig. 16. These relationships can potentially be explained by the increase in roughness, see Fig. 15(b), as a rougher tumor has a higher variance in its radius and this is what the relative shape measurements are built upon. However, it should be noted that the dependence is weak and contains large variations, especially for higher velocities.

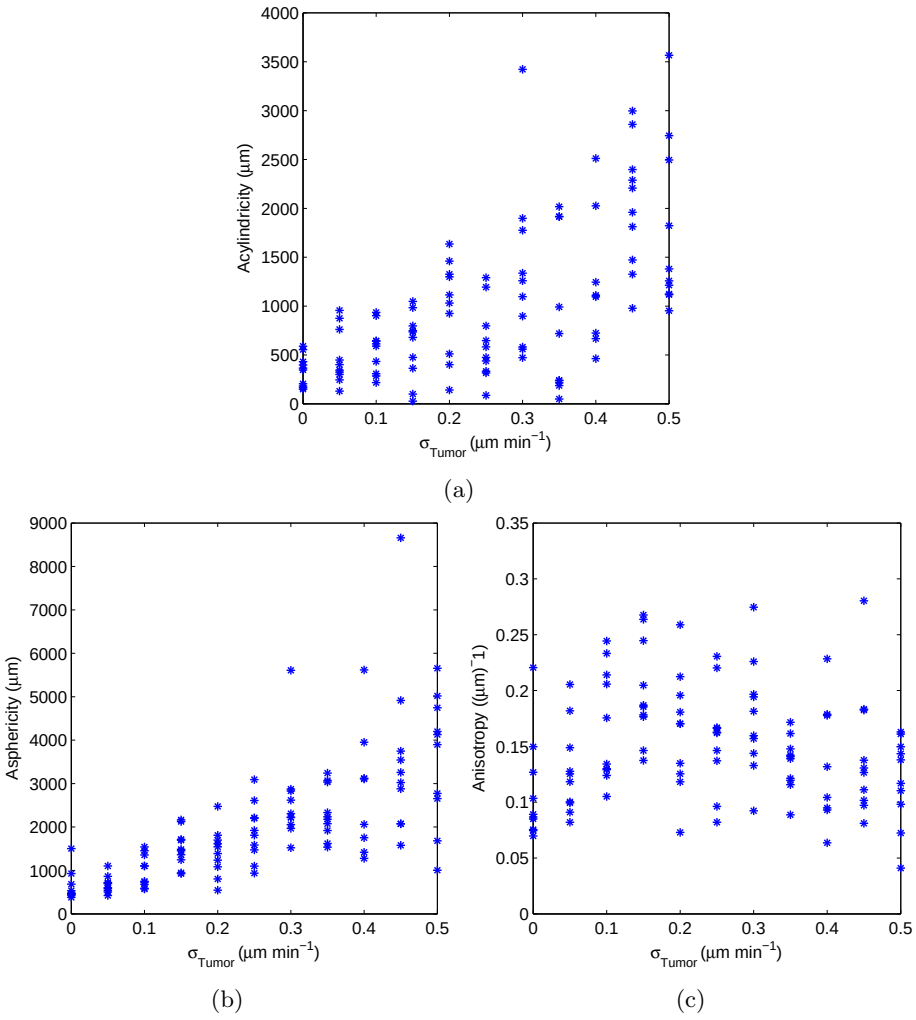

Figure 16: The dependence of the tumor velocity standard deviation on (a) acylindricity, (b) asphericity and (c) relative anisotropy. All measurements taken at size 3000 before CTL response.

Previously, the number of single cells for the different velocities has been discussed, and this analysis can be expanded looking at the distribution of cells in different sized clusters (Fig. 17). The number of single cells increases heavily with the tumor velocity standard deviation due to their ability to move. The relationship appears to be linear and increasing from $\sigma_{\text{Tumor}} = 0.1$ μm min^{-1}. Clusters of size lager than seven tumor cells behave in a similar but inverse way starting at 90-95% at σ_{Tumor} =0-0.1 μm min^{-1}. The proportion of large clusters remains dominant. The distribution of clusters of two and three cells appear to increase until they reach $\sigma_{\text{Tumor}} = 0.3$ μm min^{-1}, where they become constant or very slightly increasing. The number of cells in clusters of between four and seven cells seems to be almost constant throughout the whole simulation. The general trend seems to indicate that the higher the tumor velocity standard deviation the smaller the clusters. This causes more cells to travel in singlets and fewer cells in larger clusters. This, together with results of Fig. 10 implies that the CTL responses are more effective against large clusters of tumor cells. This is an important trade-off, which indicates that CTL responses should be well timed to tumor growth: a too early or too late response can be ineffective [12, 19].

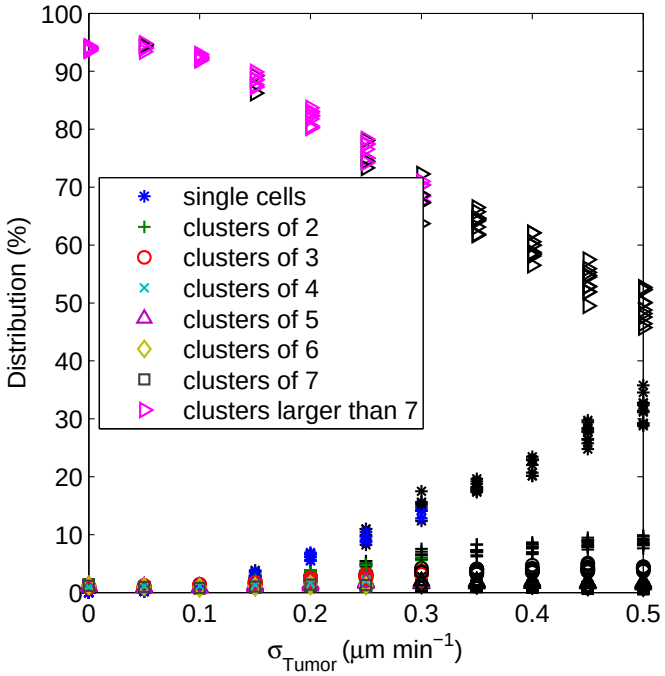

Figure 17: The distribution of cells in different sized clusters as a function of the tumor velocity standard deviation. Black symbols show cases where the CTLs are unsuccessful in eradicating the tumor. All measurements taken at size 3000 before CTL response.

To determine what effect these measures have on the time to extinction, we evaluated it as a function of different shape indicators. No general correlation could be seen, Fig. 18. However, from studying the plots carefully it can be assumed that the time to extinction is independent of a change in the density and the roughness, Fig. 18(a)-(b). The radius of gyration and the density seems to have very little variability when only larger clusters are included, but varies greatly when all tumor cells are taken into account. This indicates that the internal core is of the same size independently of the velocity, and therefore that the single cells are spread around it and these are in turn dependent on the velocity, Fig. 18(c)-(d).

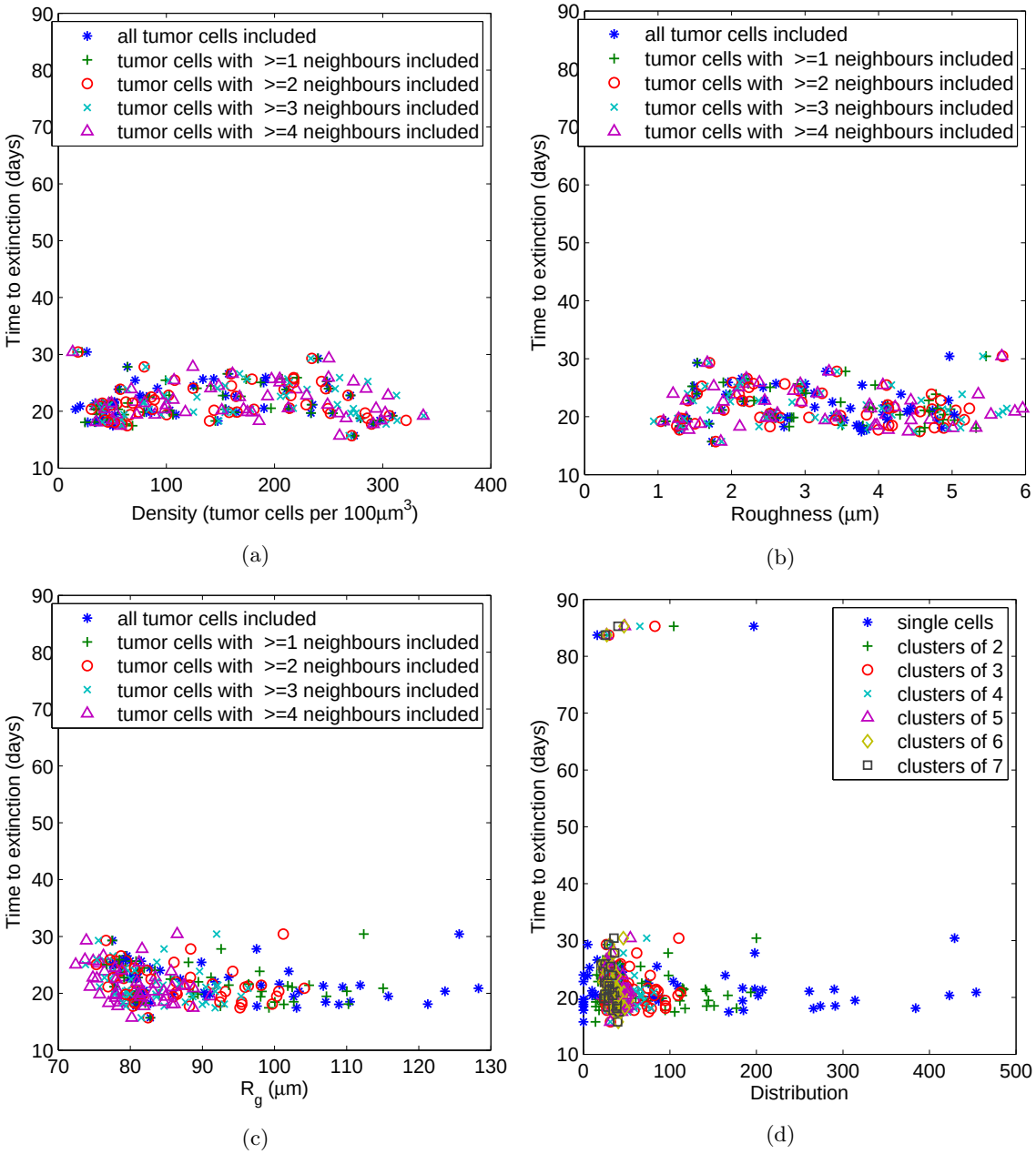

Figure 18: Time to extinction for a CTL response started at tumor size 3000 as a function of (a) density, (b) roughness, (c) radius of gyration and (d) distribution. All measurements taken at tumor number 3000 before CTL response. Different σ_{Tumor} are considered.

Finally the correlation between the time to extinction was investigated as a function of the tumor velocity standard deviation. Only simulations with a successful CTL response were taken into account. Results indicate that, except for some few examples with a higher time to eradication due to relapse, the time to eradication is constant and generally between 15-30 days. However, no tumors with a tumor velocity standard deviation higher than $\sigma_{\text{Tumor}} = 0.3\ \mu\text{m min}^{-1}$ have been eradicated.

If we look at tumor survival rates, a threshold could be identified in the area of the highest variability, separating eradication from escape. Table 1 suggests that there is a high probability of the CTL attack being successful if the density is higher than 40 tumor

cells per 100 μm^3, but a very low chance if it is lower. In regard to the roughness and radius of gyration, thresholds have values 5μm and 110 μm, below which the tumor is more likely to die. This is also the case for the distribution of single cells: when there are fewer than 12% of the total and more than 70% cells in large clusters, the result is likely to be positive. The thresholds are not completely sharp and there is an overlap around the critical values. There is also a couple of simulation result which, despite shape measurements suggest that the CTL attack would succeed, shows escape. It is important to note that these simulations have been executed during a set amount of time (200 days) and we do not take into account what happens after this time is reached.

These results differ a lot from results from the previous model where tumor movement is not taken into account. Previous results indicate that the tumor always will get eradicated on a long time scale. The new results stress how this is no longer the case when the tumor cells are motile. The outcome is now instead dependent on how fast the tumor cells are moving.

Table 1: **Table of parameters for the ABM and DDE model and estimated values.**

Quantity	Threshold	Kill under threshold (%)	Kill over threshold (%)
Density (tumor cells per 100 μm^3)	40	14	90
Roughness (μm)	5	74	10
R_g (μm)	110	84	15
Proportion of single cells (%)	12	72	9
Proportion of clusters larger then 7 (%)	70	4	84

3.4 Tumor adhesion and shape dependence on immunotherapy outcome

We now discuss the effect of adhesion. First of all, the Metropolis algorithm accepts a move with probability $p = min\left(1, e^{-\left(\sum_{i<j}(V_{ij}(t+\Delta t)-V_{ij}(t)\right)/F_T}\right)$. After adjusting the magnitude of the cell-to-cell adhesion coefficient, the probability distribution from the Metropolis algorithm of a successful trial is clearly changed. The distribution becomes narrow for low adhesion, which suggests higher probability that a move is accepted, whereas for higher adhesion it becomes wider and the tumor cells have higher probabilities of staying together. The role of the cell-to-cell adhesion is not fully understood. As such, its importance, upon eradication of a tumor, is investigated. To determine the effect of the adhesion coefficient, all simulations are performed for a tumor velocity standard deviation where the outcome is known to be positive, specifically $\sigma_{\text{Tumor}} = 0.15$ μm min^{-1}. A higher adhesion coefficient is associated with a lower probability of eradication of the tumor, as in Fig. 19. Under $\epsilon_{CCA} = 2 \cdot 10^{-16}$ m^2 kg s^{-2} the outcome is eventually eradication for every simulation. Above this value, there is a high variability in the outcome of the simulations. In a tumor with high adhesion the cells packed very close to each other, and this makes it grow extremely slow, leading to fewer antigens produced and thereby making detection for the CTLs harder. It is also more difficult for the CTLs to penetrate the tumor, therefore increasing the chance of escape. Note that eradication, both with and without relapse, is present for all different adhesion coefficients, and a successful eradication is generally more probable than tumor escape for all adhesions. This is due to the tumors low velocity making escape more difficult. The eradication probability dependent on the adhesion coefficient looks very different from the same plot for tumor velocity dependence, where

there is a clear threshold above which tumor escape is unavoidable.

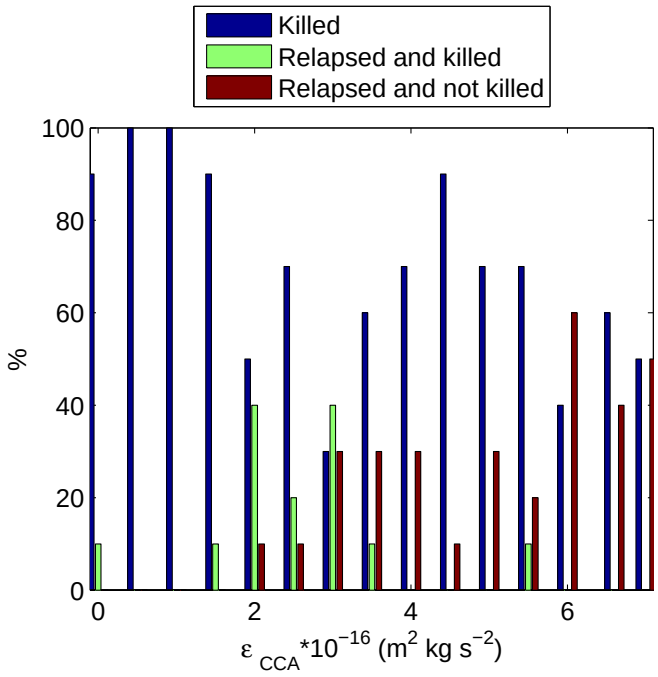

Figure 19: Histogram displaying the occurrence of different outcomes as a function of adhesion coefficient. CTL response starts at 3000 tumor cells.

The influence of the adhesion coefficient on the shape is very different from the effects due to the tumor velocity standard deviation, and it is characterized by an overall higher variability, see Fig. 20. The density seems to be almost constant up to $\epsilon_{CCA} \approx 2.5$ m^2 kg s^{-2} where the density becomes highly variable and starts to increase heavily and non linearly, see Fig. 20(a). The roughness increases up to a maximum at around $\epsilon_{CCA} = 2 - 3$ m^2 kg s^{-2} and then starts to decrease before reaching a low constant value over $\epsilon_{CCA} = 5$ m^2 kg s^{-2}, see Fig. 20(b). Similarities can be found in the radius of gyration, which is decreasing with the adhesion coefficient but has a steeper slope between $\epsilon_{CCA} = 2$ m^2 kg s^{-2} and $\epsilon_{CCA} = 3.5$ m^2 kg s^{-2}, Fig. 20(c). As apparent in Fig. 20(d), there is a pronounced inverse non linear correlation between the growth speed of the tumor and the adhesion coefficient. This together implies that the tumor is more compact and there is insufficient room for division for a number of the tumor cells.

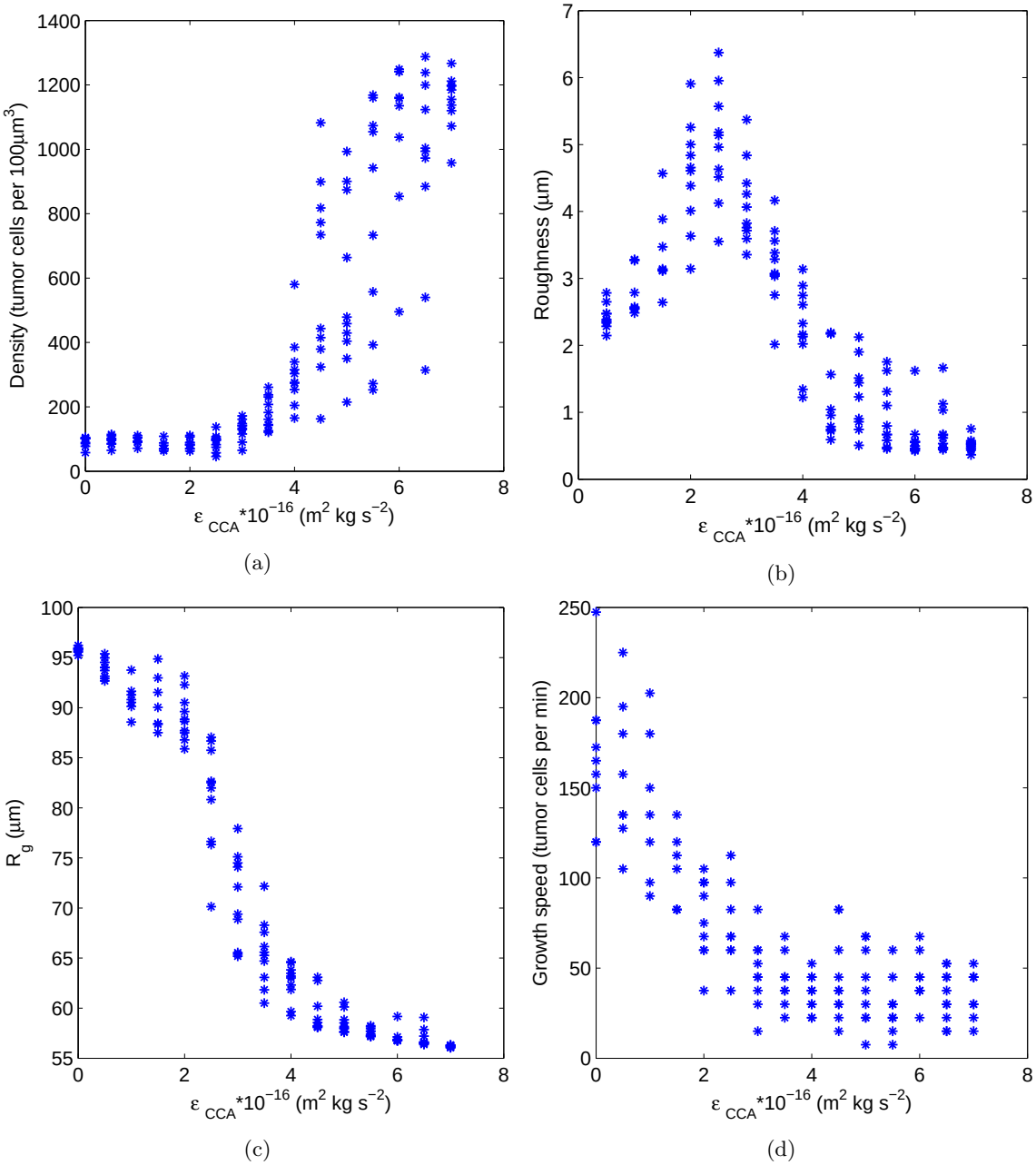

Figure 20: The effect of the adhesion coefficient for a tumor just before the CTL response at tumor size 3000 on (a) density, (b) roughness, (c) radius of gyration and (d) tumor number growth speed. Note that a fixed $\sigma_{tumor} = 0.15$ μm min^{-1} is used. These results are generally dependent on the tumor velocity.

Investigation of the cell-to-cell adhesion coefficient on the relative shape measurements indicated that a dependence is hard to determine, see Fig. 21. The asphericity and relative shape anisotropy behave in a similar way to the roughness and show an increase until reaching a maximum $\sigma_{tumor} = 2 - 3$ m^2 kg s^{-2}, after which decrease. However, it should be noted that there is high variability in the results.

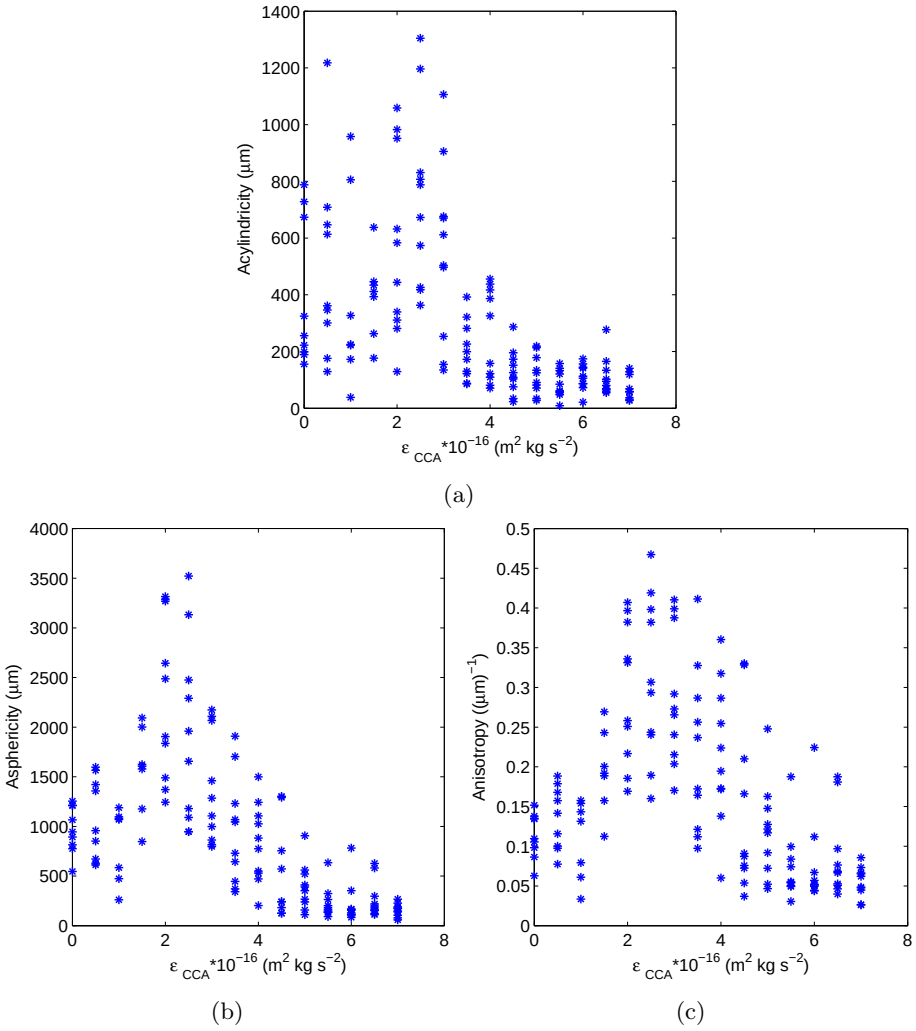

Figure 21: The dependence of the adhesion coefficient on (a) acylindrisity, (b) asphericity and (c) relative anisotropy. All measurements taken at size 3000 before CTL response.

It is very interesting to look at the distribution of cell clusters as functions of the adhesion coefficient, Fig 22. It looks very different from the distribution plot from the tumor velocity standard deviation: the dependence is inverted. This is due to the fact that the higher the adhesion coefficient, the greater the likelihood that the tumor stays in large clusters. Based upon the same argument used above for the tumor velocity, this suggests the tumor is more likely to be killed. However, this is not the case and may be due to a limitation in the shape measurements. The shape measurements do not take into account several small tumors, but rather approximate them all into one collective radius. When the tumor consists of many small very dense tumors the result can be very slow tumor growth leading to inability of the CTL response to detect the tumor quickly enough. In tumors with higher adhesion almost all cancer cells belong to clusters larger than seven cells. This is consistent with results by Kim et al. [19] regarding slow growing tumors.

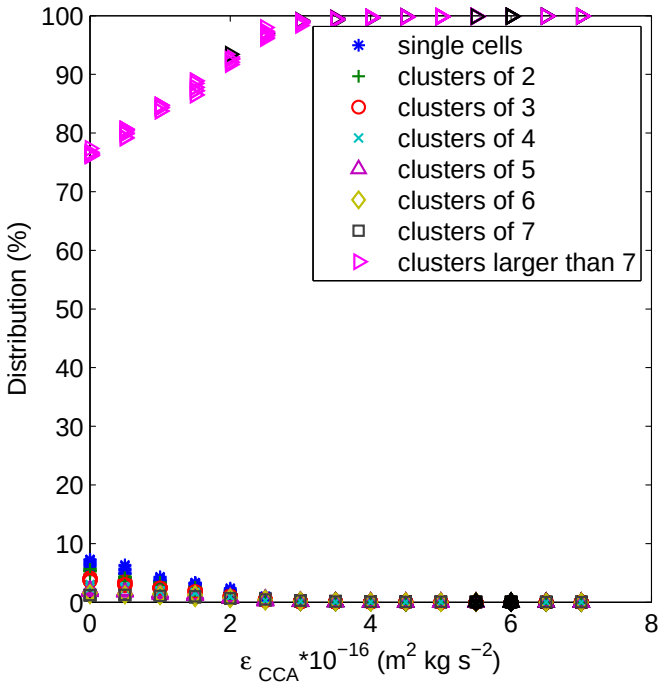

Figure 22: Growth speed of the tumor as a function of tumor standard deviation when all tumor cells are included for a CTL response started at tumor size 3000.

Further analysis of the shape measures reveals a dependence on the time to eradication, Fig. 23. It is interesting to note that for many of the simulations the shape is the same independently of how many neighbors are required to be included; this indicates that most of the cells have several neighbors. The density varies greatly for different simulations. For low densities the time to eradication is clearly shorter than for high densities and increases fast for low velocities to reach a constant higher value Fig. 23(a). The time to eradication has an inverse, almost linear, relationship to both the roughness and radius of gyration, Fig. 23(b)-(c). A rougher tumor is, loosely speaking, easier to penetrate and therefore faster to kill. Variations in the distribution seems to have little effect on the time to eradication, except for tumors where the occurrence of singlets up to clusters of seven is zero, leaving all the tumor cells in large clusters, which induces an increase in time, Fig. 23(d). Outliers are due to relapses. These clear shape dependencies on the time to eradication differ from the variations observed for the tumor velocity.

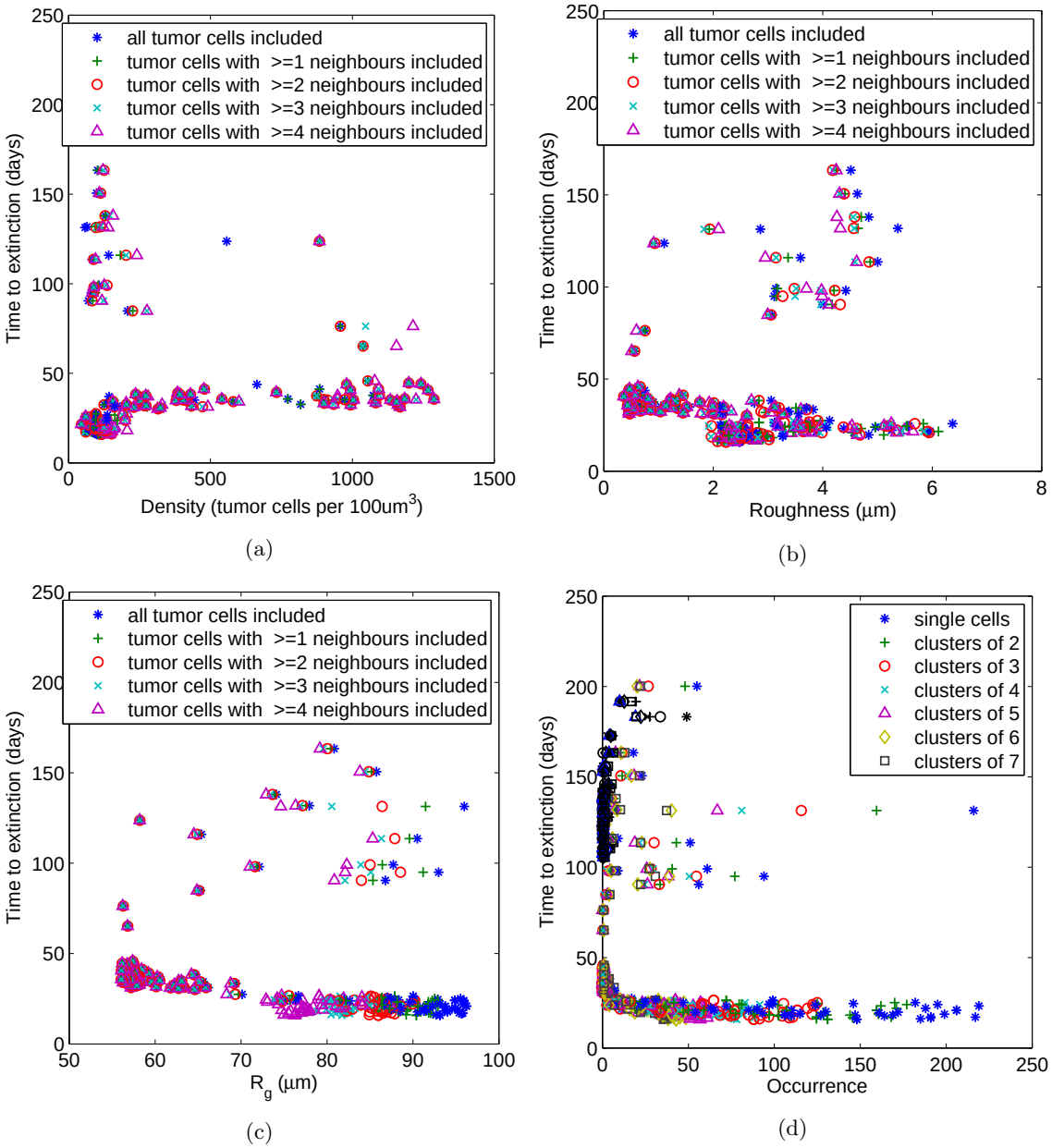

Figure 23: Time to extinction for a CTL response started at tumor size 3000 as a function of (a) density, (b) roughness, (c) radius of gyration and (d) distribution. All measurements taken at tumor size 3000 cells before CTL response is initiated.

Looking at the time to eradication directly dependent on the adhesion coefficient, a constant time, around 20 days, for adhesion coefficients up to $\epsilon_{CCA} = 2.5$ m^2 kg s^{-2} is observed. Then a sudden increase up to 30 days occurs and the data become constant again, Fig. 24. Note that this is the same value that was found both in the roughness, radius of gyration and the relative shape measurements, where shape changes occur (see Fig. 20). It seems $\epsilon_{CCA} \approx 2.5$ m^2 kg s^{-2} is a "critical" point, where the effects of high adhesion and velocity made tumors harder to destroy. Tumors with low adhesion are spread but uniform, due to their inability to stick to each other, so that the velocity assumes a dominant role in making the cancer difficult to chase. Tumors with high adhesion become very dense and spherical due to the dominance of the adhesion over the velocity. Instead, at average

values of adhesion, specifically at around $\epsilon_{CCA} = 2.5$ m^2 kg s^{-2}, tumors are effected by both the adhesion and the velocity leading to cancers instead forming several dense lumps, giving rise to peaks in Fig. 24. The existence of a dependence of the adhesion coefficient on the time to eradication is different to the corresponding results from the tumor velocity. There is also no threshold after which escape is unavoidable. The outliers are results from tumors with one or several relapses.

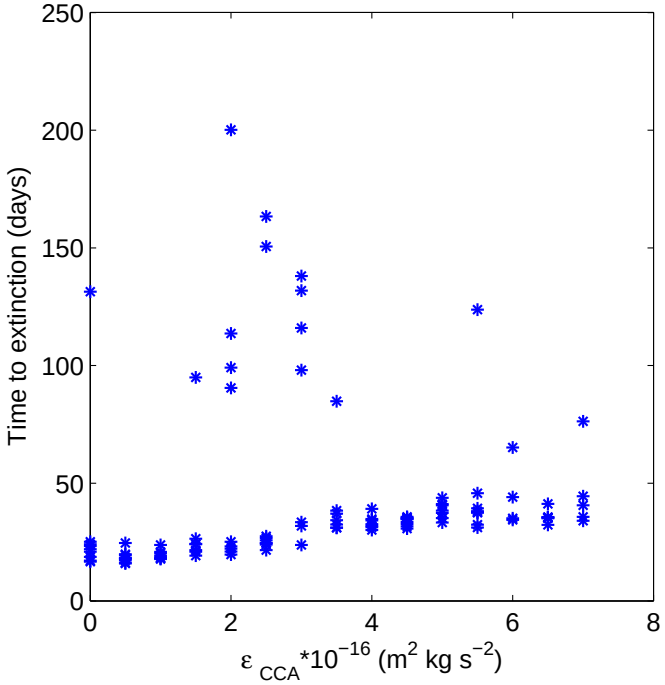

Figure 24: Time to eradication as a function of cell-to-cell adhesion coefficient when all tumor cells are included for a CTL response started at tumor size 3000. For this value of σ_{tumor}, $\epsilon_{CCA} \simeq 2.5 \cdot 10^{-16}$ m^2 kg s^{-2} causes the tumor to be particularly aggressive and hard to eradicate.

Applying similar analysis as for the tumor velocity, different shape measurements leads to a much weaker and shifted thresholds, as indicated in table 2. This means, as discussed above, that shape measurements are not always faithful indicators of outcomes, especially when different ϵ_{CCA} are considered.

Table 2: **Table of parameters for the ABM and DDE model and estimated values.**

Quantity	Threshold	Kill under threshold (%)	Kill over threshold (%)
Density (tumor cells per 100 μm^3)	1000	84	56
Roughness (μm)	3.5	78	82
R_g (μm)	75	66	96
Proportion of single cells	3	71	100
Proportion of clusters larger then 7	95	98	69

Interestingly, when using a higher velocity, $\sigma_{tumor} = 0.25$ μm min^{-1}, the adhesion coefficient seems to have little effect on the outcome of the result. The combination of high

velocity and high adhesion leads to a very unpredictable outcome. These results indicate that a tumor where the cells move fast will be very hard to kill, independent of the cell-to-cell adhesion. If the tumor velocity is lower, the adhesion has some impact on the result but with high variability.

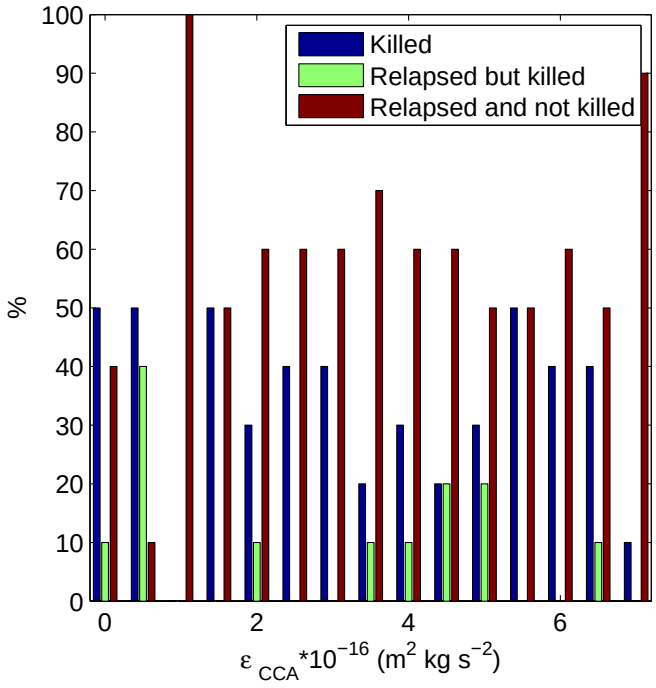

Figure 25: Histogram displaying the occurrence of different outcomes as a function of adhesion coefficient with $\sigma_{tumor} = 0.25$ μm min^{-1}. CTL response starts at tumor size 300 cells. Note the degree of unpredictability when this figure is compared with previous histograms.

3.5 Size dependence

It is also interesting to look at the time to extinction as a function of tumor size. Simulations have been performed once for low ($\sigma_{tumor} = 0.1$ μm min^{-1} and $\epsilon_{CCA} = 1.5$ m^2 kg s^{-2}) and once for high ($\sigma_{tumor} = 0.2$ μm min^{-1} and $\epsilon_{CCA} = 3$ m^2 kg s^{-2}) tumor velocity and adhesion, Fig. 26. The time to extinction is almost constant for the different simulations once the tumor is larger than 2000 cells. Before this size is reached, the eradication time is longer and the variability higher. This behavior originates from the CTLs having difficulty detecting the tumor and commencing eradication. This is very similar for both parameter sets, however, if studying the figures closely, a slight increase in time to eradication with tumor number can be noted for the lower parameter set. Note that the outliers, above time 60 days, are tumors that have relapsed once and, above around 150 days, twice. These latter bands resemble the lower bands, but with a greater spread. There are more tumors that have relapsed for the lower sizes. This therefore suggests that it is easier to eradicate tumors that are slightly larger. This supports conclusions drawn in chapter 3.4 regarding high adhesion tumors. In some cases (black symbols) the tumor has not been eradicated.

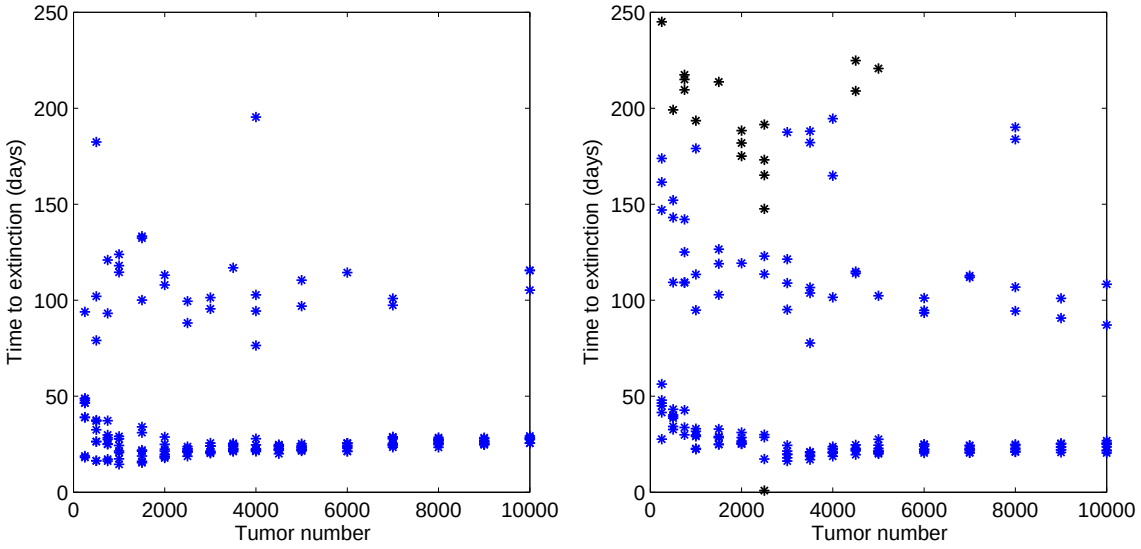

(a) (b)

Figure 26: Time to eradication as a function of tumor size for (a) $\sigma_{tumor} = 0.1$ μm min^{-1} and $\epsilon_{CCA} = 1.5$ m^2 kg s^{-2} and (b) $\sigma_{tumor} = 0.2$ μm min^{-1} and $\epsilon_{CCA} = 3$ m^2 kg s^{-2}.

3.6 Investigation of growth and eradication trends

Matlab function "nlinfit" is used to fit both an exponential and a power law to the tumor population, as a function of time. This examination is performed for one simulation with standard parameters and results are similar for other cases. The adhesion and velocity is then increased and decreased separately. It is apparent in Figs. 27-28 that the tumor does not grow exponentially for standard parameters, nor in the cases of low velocity (Fig. 28(a)) or high adhesion (Fig. 28(d)). Power curves are almost overlapping and can be assumed to be the best fit and a higher adhesion coefficient leads to a considerably slower growth. The same behavior can be seen for low velocity. In the case of low adhesion (Fig. 28(c)) and high velocity (Fig. 28(b)) the exponential curve becomes a better approximation but is still not the best fit. Jeon et al. have suggested that the radius of the tumor and the total cell count, N_c, is related by $rN_c^{1/d}$ where d is the dimensionality and r the radius [14]. This leads to the conclusion that the radius of the tumors is growing almost linearly when the tumor has a high adhesion or low velocity and the faster the tumor cells move (or the lower adhesion) the more similar is the growth to an exponential growth. This is in agreement with results in section 3.3. The values of the coefficients for the curves chosen can be found in Table 3.

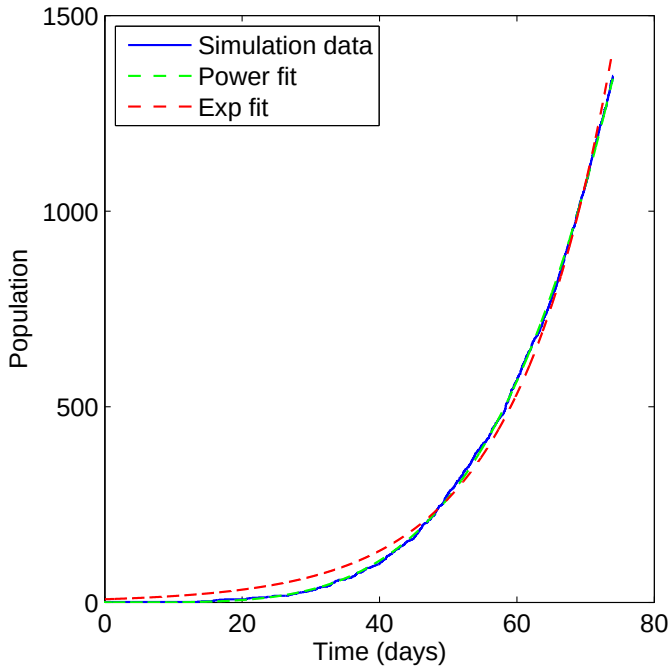

Figure 27: Growth speed of the tumor as a function of tumor standard deviation for $\sigma_{tumor} = 0.15$ μm min^{-1} and $\epsilon_{CCA} = 1.5$ m^2 kg s^{-2} when all tumor cells are included for a CTL response started at tumor size 3000.

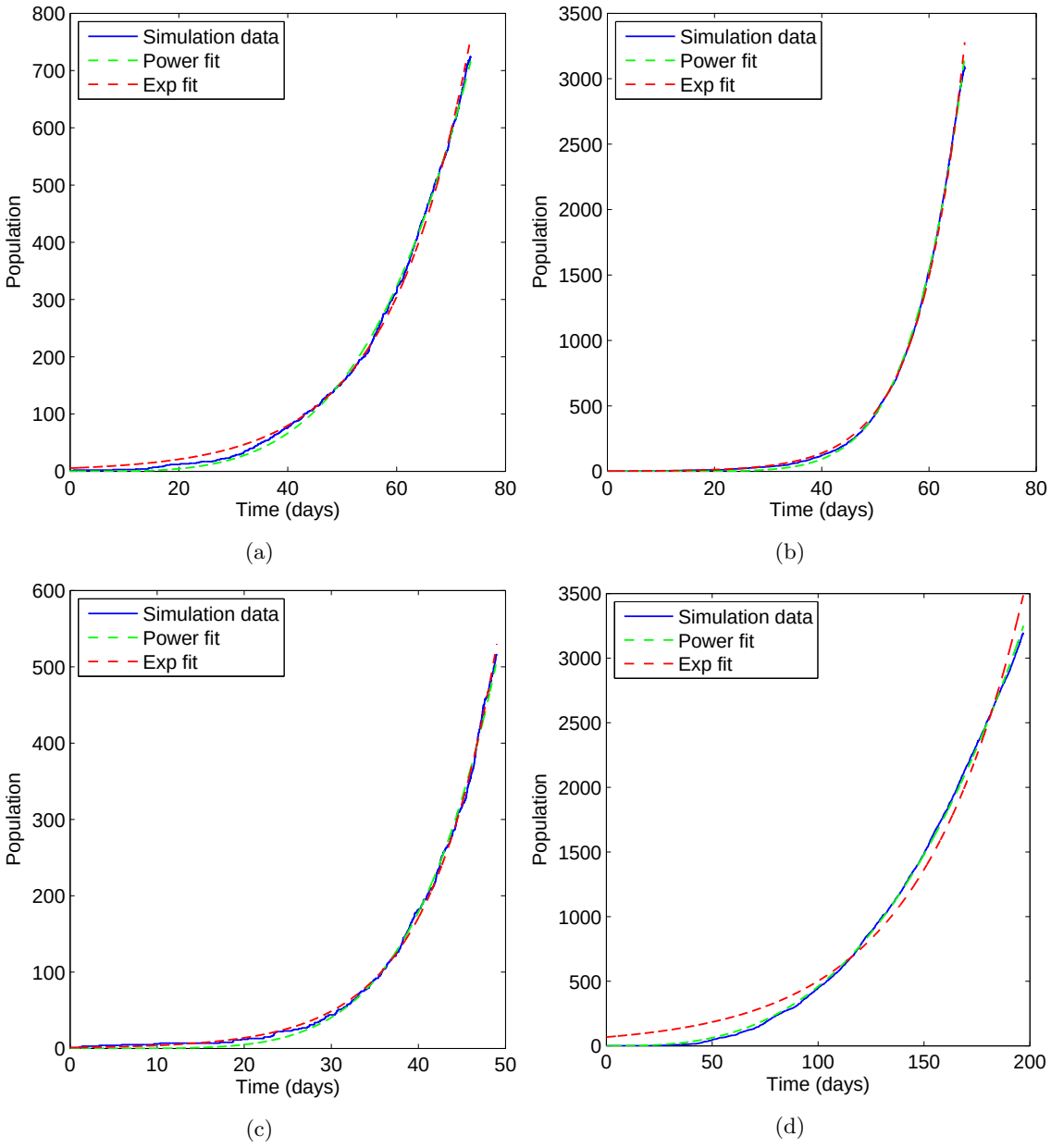

Figure 28: Growth speed of the tumor as a function of tumor standard deviation for (a) $\sigma_{tumor} = 0.05$ μm min^{-1} and $\epsilon_{CCA} = 1.5$ m^2 kg s^{-2}, (b) $\sigma_{tumor} = 0.35$ μm min^{-1} and $\epsilon_{CCA} = 1.5$ m^2 kg s^{-2}, (c) $\sigma_{tumor} = 0.15$ μm min^{-1} and no ϵ_{CCA} and (d) $\sigma_{tumor} = 0.15$ μm min^{-1} and $\epsilon_{CCA} = 6.5$ m^2 kg s^{-2}. All tumor cells are included and for a CTL response started at tumor size 3000.. All tumor cells are included and for a CTL response started at tumor size 3000.

Table 3: **Table with fitted curves and corresponding Mean Square Error (MSE) for growth.**

σ_{tumor} (μm min^{-1})	$\epsilon_{CCA} \cdot 10^{-16}$ (m^2 kg s^{-2})	Power function:	MSE	Exp function:	MSE
0.15	1.5	$y(t) = 2.71 \cdot 10^{-5} \cdot t^{4.11}$	25	$y(t) = 8.05 \cdot e^{0.07t}$	621
0.05	1.5	$y(t) = 3.78 \cdot 10^{-5} \cdot t^{3.90}$	45	$y(t) = 5.50 \cdot e^{0.07t}$	95
0.35	1.5	$y(t) = 8.05 \cdot 10^{-10} \cdot t^{6.91}$	283	$y(t) = 1.21 \cdot e^{0.12t}$	442
0.15	0	$y(t) = 9.95 \cdot 10^{-7} t^{5.15}$	19	$y(t) = 1.13e^{0.13t}$	33
0.15	6.5	$y(t) = 0.0008 \cdot t^{2.89}$	352	$y(t) = 67.69 \cdot e^{0.02t}$	$1.23 \cdot 10^4$

3.7 Parameters used in this thesis

The maximum simulation time is set to 200 days for most of the cases, but 300 days for the investigation of the adhesion dependence have been allowed (the latter due to the slow growth of high adhesion tumors). This is both for computational reasons and for the initial assumption on describing only solid micro tumors. If the tumors grow larger, parameters and assumptions used in the model might be inaccurate. While the model is not focusing on the chance for extinction on a longer time scale, it can instead be seen as the probability of extinction within the time frame for the tumor to remain of a moderate size.

Same parameters have been used by Kim et al. [19], see Table 4, whereas new parameters added for the tumor cell motility are also used.

The cut-off distance for the cell-to-cell repulsion is estimated to be given by cells touching each other, $r_{cut}^{CCR} = 2r$. For adhesion, $r_{cut}^{CCA} = 3r$, which translates into a distance between the cells of one cell radius. This is based on work performed by Jeon et al. [14] and Frascoli et al. [24]. The cell-to-cell repulsion and adhesion coefficients are chosen to be in the same ranges as the reference energy, $\epsilon^{CCR} = 1.5 \cdot 10^{-16}$ m^2 kg s^{-2}, $\epsilon^{CCA} = (0-7) \cdot 10^{-16}$ m^2 kg s^{-2}, which is also in good agreement with Jeon et al. Drasdo et al. [38] suggest that the reference energy for cells lies between $F_T = 2 \cdot 10^{-15}$ J, [48], and $F_T = 10^{-17}$ J, [47]: for this reason we choose a reference energy in between the two extremes: $F_T = 10^{-16}$ J. The cell speed is not universally determined and it has been suggested by Sahai et al. [17] to be between 0.1-1 μm min^{-1}. This range is examined.

Table 4: **Table of parameters for the ABM and DDE model and estimated values.**

Parameter	Description	Estimate (Range)
Δt	Time-step	1 min
r	Radius of cells	5 μm
T_{div}	Avg. division time of tumor cell	7 days
σ_{CTLmax}	Max unit standard deviation of CTL diffusion	12μm/min
C_{acc}	CTL acceleration time from 0 to σ_{CTLmax}	5 h
C_{death}	Avg. CTL lifespan	41 h
C_{recruit}	Avg. time for CTL recruitment	8 h
C_{kill}	Avg. time for CTL to kill tumor cell	24 h
R	Radius of region of interest	620.4 μm
h	Thickness of CTL cloud	$3\sigma_{\text{CTLmax}}\sqrt{\Delta t}$
V_{ratio}	Ratio of volume of tissue to the lymph node	1000
$A_0(0)$	Initial concentration of immature APCs	0.01 k/mm^3
d_0	Death/turnover rate of immature APCs	0.03 day^{-1}
s_A	Supply rate of immature APCs	$A_0(0)d_0 = 0.3$ k/mm^3 day^{-1}
d_1	Death/turnover rate of mature APCs	0.8 day^{-1}
K	Initial/equilibrium concentration of memory CTLs	$2\% \cdot 200$ k/mm^3
r	Logistic growth rate of memory CTLs	0.7 day^{-1}
m	Minimal number of CTL divisions	10 (7–17)
δ_1	Death/turnover rate of effector CTLs	0.4 day^{-1}
μ	Mass-action coefficient	20(k/mm^3)$^{-1}$ day^{-1}
ρ	Duration of one CTL division	1/3 day
σ	Duration of CTL division program	$1 + (m-1)\rho$
α	Antigenicity of the tumor	10^{-9}
f	CTLs flow rate out of lymph node to tissue	0.7 day^{-1}
r_{cut}^{CCA}	Cut of radius for the Cell-Cell adhesion	$1.5 \cdot 2r$
ϵ_{CCA}	Cell-Cell adhesion force coefficient	$1.5 \cdot 10^{-16}((0-7) \cdot 10^{-16})$ m^2 kg s^{-2}
r_{cut}^{CCR}	Cut of radius for the Cell-Cell repulsion	$2r$
ϵ_{CCR}	Cell-Cell repulsion force coefficient	$3 \cdot 10^{-16}$ m^4 kg s^{-2}
F_T	Reference energy	10^{-16} J
σ_{tumor}	Tumor standard deviation	0.15 (0-5) μm min^{-1}
ρ	CTL compressibility	50%
α_c	Tumor cell compressibility	40%

4 Conclusions

In the development of an effective vaccine against cancer it is important to understand the interaction between the immune response and the tumor cells. We have simulated this and investigated the effect of different parameters on the outcome of an immune response to a tumor growth. From the previous chapters we can extract some general conclusions about this study. The former model always lead to extinction of the tumor, our addition of motility to the tumor cells changed that conclusion. When looking at results from different simulations the outcome can seem random. There is a high variance in some results and a lower one in others. Despite this, we ask the important question: is it possible to predict the outcome?
The outcome from an immunotherapy against cancer is strongly dependent on the velocity of the tumor cells. A high velocity leads, in almost every case, to a relapse and tumor escape. The tumor velocity, in turn, affects the shape and especially the number of cells that travel in clusters by themselves. This leads to a high spread of the tumor. These kinds of shapes are possible to be investigated clinically and can therefore lead to a conclusion about the outcome of a potential vaccination. Tumors where the cell speed is lower, tend to stay in more uniform shapes and larger clusters, giving the immune response a better chance of detection and total eradication.

It is more difficult to figure out a trend for the dependence upon the adhesion, since it has very high variability. However, the general trend shows that tumor cells with low adhesion tend to create a high number of single cells, which, together with a high velocity, makes relapse probable. If the tumor cells have low velocity the tumor grows fast, gets detected and has higher probability of getting eradicated without relapse. When tumor cells experience high adhesion, they favor staying close together which leads to a more compact tumor where growth is very slow. This leads to a tumor that easily goes unnoticed from the immune response, and the longer the delay in the response, the likelier it is that one tumor cell migrates away. When the immune response finally detects this highly dense tumor, the time to eradicate it is longer since the CTLs have difficulties penetrating the tumor and kill cells only on the surface. This insight is also supported by size dependence measurements, which imply that small tumors are more difficult to detect and take longer for the immune system to eradicate. When the velocity is higher, a change in the adhesion has less impact: high adhesion follows the same behavior as for a low velocity tumor, however, low adhesion leads to a very spread tumor, where one or more tumor cells often escapes, subsequently causing relapse.

These conclusions give good ranges for possibility of unsatisfactory result: a tumor consisting of almost only single cells will be very difficult to kill, but, at the same time, no cells in small clusters suggest a very high adhesive force, making detection and penetration difficult. A tumor with any of these properties will prove very hard to destroy. It is also interesting how a particular combination of tumor velocity and adhesion creates an extremely rough tumor consisting of several lumps leading the transition from a higher probability of eradication to a considerably lower one.

Both velocity and adhesion have a great effect on the growth speed of a tumor, which was found to be slower than linear for high adhesion and changes considerably for high velocity and low adhesion tumors.

This model is based on simple but established assumptions. The tumor interactions are based on solely adhesion and repulsion, and an inclusion of chemotaxis is interesting for future studies. A way of making the model more realistic would also be to include nutrition dependence for the tumor. Another limitation of the model is the inability of

creating tumors of varying shapes without changing any parameter. Devising a method for generating arbitrary shapes would also be an important advancement.

These findings and future mathematical models of the type discussed in this thesis will inform detection, diagnostics and treatment necessary for effective cancer therapy. Beyond the immediate applications for cancer therapy, our results provide insight into fundamental understanding of biology and the influence of velocity/adhesion upon cell behavior.

Overall, this study shows that preventative cancer vaccines have a good potential for the future. It also identifies tumor velocity as an important factor in cancer treatment and, as such, its study in future research is fundamental to maximize the benefits of immunotherapy techniques.

References

[1] R. Siegel, D. Naishadham, and A. Jemal, "Cancer statistics, 2013," *CA Cancer J. Clin.*, vol. 63, no. 1, pp. 11–30, 2013.

[2] A. M. Stein, T. Demuth, D. Mobley, M. Berens, and L. M. Sander, "A mathematical model of glioblastoma tumor spheroid invasion in a three-dimensional in vitro experiment," *Biophys. J.*, vol. 92, no. 1, pp. 356–365, 2007.

[3] F. O. Nestle, G. Tonel, and A. Farkas, "Cancer vaccines: the next generation of tools to monitor the anticancer immune response," *PLoS med.*, vol. 2, no. 10, p. e339, 2005.

[4] C. Yee, J. Thompson, D. Byrd, S. Riddell, P. Roche, E. Celis, and P. Greenberg, "Adoptive t cell therapy using antigen-specific cd8+ t cell clones for the treatment of patients with metastatic melanoma: in vivo persistence, migration, and antitumor effect of transferred t cells," *PNAS*, vol. 99, no. 25, pp. 16168–16173, 2002.

[5] M. E. Dudley, J. R. Wunderlich, P. F. Robbins, J. C. Yang, P. Hwu, D. J. Schwartzentruber, S. L. Topalian, R. Sherry, N. P. Restifo, A. M. Hubicki, *et al.*, "Cancer regression and autoimmunity in patients after clonal repopulation with antitumor lymphocytes," *Science*, vol. 298, no. 5594, pp. 850–854, 2002.

[6] H. Greenspan, "Models for the growth of a solid tumor by diffusion," *Stud. Appl. Math*, vol. 51, no. 4, pp. 317–340, 1972.

[7] T. Roose, S. J. Chapman, and P. K. Maini, "Mathematical models of avascular tumor growth," *Siam Rev.*, vol. 49, no. 2, pp. 179–208, 2007.

[8] N. Bellomo, N. Li, and P. K. Maini, "On the foundations of cancer modelling: selected topics, speculations, and perspectives," *M3AS*, vol. 18, no. 04, pp. 593–646, 2008.

[9] A.-S. Qi, X. Zheng, C.-Y. Du, and B.-S. An, "A cellular automaton model of cancerous growth," *J. Theor. Biol.*, vol. 161, no. 1, pp. 1–12, 1993.

[10] D. G. Mallet and L. G. De Pillis, "A cellular automata model of tumor–immune system interactions," *J. Theor. Biol.*, vol. 239, no. 3, pp. 334–350, 2006.

[11] A. Mogilner, "Mathematics of cell motility: have we got its number?," *J. math. biol.*, vol. 58, no. 1-2, pp. 105–134, 2009.

[12] F. Frascoli, B. D. Hughes, M. H. Zaman, and K. A. Landman, "A computational model for collective cellular motion in three dimensions: General framework and case study for cell pair dynamics," *PloS one*, vol. 8, no. 3, p. e59249, 2013.

[13] E. A. Codling, M. J. Plank, and S. Benhamou, "Random walk models in biology," *J. R. Soc. Interface*, vol. 5, no. 25, pp. 813–834, 2008.

[14] J. Jeon, V. Quaranta, and P. T. Cummings, "An off-lattice hybrid discrete-continuum model of tumor growth and invasion," *Biophys. J.*, vol. 98, no. 1, pp. 37–47, 2010.

[15] G. Landini and J. Rippin, "How important is tumour shape? quantification of the epithelial–connective tissue interface in oral lesions using local connected fractal dimension analysis," *J. Pathol.*, vol. 179, no. 2, pp. 210–217, 1996.

[16] R. M. Rangayyan, N. R. Mudigonda, and J. L. Desautels, "Boundary modelling and shape analysis methods for classification of mammographic masses," *Med. Biol. Eng. Comput.*, vol. 38, no. 5, pp. 487–496, 2000.

[17] E. Sahai, "Mechanisms of cancer cell invasion," *Curr. Opin. Genetics. Dev.*, vol. 15, no. 1, pp. 87–96, 2005.

[18] V. Narang, S. Y. Wong, S. R. Leong, J.-P. Abastado, and A. Gouaillard, "Comparing mathematical models of cell adhesion in tumors," in *Defense Science Research Conference and Expo (DSR), 2011*, pp. 1–4, IEEE, 2011.

[19] P. S. Kim and P. P. Lee, "Modeling protective anti-tumor immunity via preventative cancer vaccines using a hybrid agent-based and delay differential equation approach," *PLoS comp. biol.*, vol. 8, no. 10, p. e1002742, 2012.

[20] W. Wang, J. Epler, L. G. Salazar, and S. R. Riddell, "Recognition of breast cancer cells by cd8+ cytotoxic t-cell clones specific for ny-br-1," *Cancer Res.*, vol. 66, no. 13, pp. 6826–6833, 2006.

[21] B. Vogelstein and K. W. Kinzler, "Cancer genes and the pathways they control," *Nature med.*, vol. 10, no. 8, pp. 789–799, 2004.

[22] C. S. H. Laboratory, "Hallmarks of cancer," Oct. 2013.

[23] D. Hanahan and R. A. Weinberg, "The hallmarks of cancer," *Cell*, vol. 100, no. 1, pp. 57–70, 2000.

[24] P. Fedi, S. Tronick, and S. Aaronson, "Growth factors," *Cancer medicine*, pp. 41–64, 1997.

[25] R. A. Weinberg, "The retinoblastoma protein and cell cycle control," *Cell*, vol. 81, no. 3, pp. 323–330, 1995.

[26] A. Willie, "Cell death: the significance of apoptosis.," *Int. Rev. Cytol.*, vol. 68, pp. 251–306, 1980.

[27] G. Evan and T. Littlewood, "A matter of life and cell death," *Science*, vol. 281, no. 5381, pp. 1317–1322, 1998.

[28] L. Hayflick, "Mortality and immortality at the cellular level. a review," *Biochemistry-New York-English Translation of Biokhimiya*, vol. 62, no. 11, pp. 1180–1190, 1997.

[29] N. Bouck, V. Stellmach, and S. C. Hsu, "How tumors become angiogenic," *Adv. Cancer Res.*, vol. 69, pp. 135–174, 1996.

[30] M. B. Sporn, "The war on cancer," *Lancet*, vol. 347, no. 9012, pp. 1377–1381, 1996.

[31] J. P. Johnson, "Cell adhesion molecules of the immunoglobulin supergene family and their role in malignant transformation and progression to metastatic disease," *Cancer Metastasis Rev.*, vol. 10, no. 1, pp. 11–22, 1991.

[32] G. P. Dunn, L. J. Old, and R. D. Schreiber, "The immunobiology of cancer immunosurveillance and immunoediting," *Immunity*, vol. 21, no. 2, pp. 137–148, 2004.

[33] V. Kuznetsov, "Basic models of tumor-immune system interactions identification, analysis and predictions," in *A Survey of Models for Tumor-Immune System Dynamics*, pp. 237–294, Springer, 1997.

[34] M. H. Andersen, D. Schrama, P. thor Straten, and J. C. Becker, "Cytotoxic t cells," *J. Invest. Dermatol.*, vol. 126, no. 1, pp. 32–41, 2006.

[35] R. Soiffer, F. S. Hodi, F. Haluska, K. Jung, S. Gillessen, S. Singer, K. Tanabe, R. Duda, S. Mentzer, M. Jaklitsch, *et al.*, "Vaccination with irradiated, autologous melanoma cells engineered to secrete granulocyte-macrophage colony-stimulating factor by adenoviral-mediated gene transfer augments antitumor immunity in patients with metastatic melanoma," *J. Clin. Oncol.*, vol. 21, no. 17, pp. 3343–3350, 2003.

[36] R. Jaini, P. Kesaraju, J. M. Johnson, C. Z. Altuntas, D. Jane-Wit, and V. K. Tuohy, "An autoimmune-mediated strategy for prophylactic breast cancer vaccination," *Nature med.*, vol. 16, no. 7, pp. 799–803, 2010.

[37] A. Brú, S. Albertos, J. Luis Subiza, J. L. García-Asenjo, and I. Brú, "The universal dynamics of tumor growth," *Biophys. J.*, vol. 85, no. 5, pp. 2948–2961, 2003.

[38] D. Drasdo and S. Höhme, "A single-cell-based model of tumor growth in vitro: monolayers and spheroids," *Phys. biol.*, vol. 2, no. 3, p. 133, 2005.

[39] B. Gompertz, "On the nature of the function expressive of the law of human mortality, and on a new mode of determining the value of life contingencies," *Philos. Trans. R. Soc. London*, vol. 115, pp. 513–583, 1825.

[40] R. Berger, "Comparison of the gompertz and logistic equations to describe plant disease progress.," *Phytopathology*, vol. 71, no. 7, pp. 716–719, 1981.

[41] A. d'Onofrio, "A general framework for modeling tumor-immune system competition and immunotherapy: Mathematical analysis and biomedical inferences," *PHYD*, vol. 208, no. 3, pp. 220–235, 2005.

[42] P. Dieterich, R. Klages, R. Preuss, and A. Schwab, "Anomalous dynamics of cell migration," *PNAS*, vol. 105, no. 2, pp. 459–463, 2008.

[43] J. C. Mombach and J. A. Glazier, "Single cell motion in aggregates of embryonic cells," *Phys. Rev. Lett.*, vol. 76, no. 16, p. 3032, 1996.

[44] P. N. Devreotes and S. H. Zigmond, "Chemotaxis in eukaryotic cells: a focus on leukocytes and dictyostelium," *Annu. Rev. Cell Biol.*, vol. 4, no. 1, pp. 649–686, 1988.

[45] N. Metropolis, A. W. Rosenbluth, M. N. Rosenbluth, A. H. Teller, and E. Teller, "Equation of state calculations by fast computing machines," *J. Chem. Phys.*, vol. 21, p. 1087, 1953.

[46] D. Drasdo, R. Kree, and J. McCaskill, "Monte carlo approach to tissue-cell populations," *Phys. Rev. E*, vol. 52, no. 6, p. 6635, 1995.

[47] M. Schienbein, K. Franke, and H. Gruler, "Random walk and directed movement: comparison between inert particles and self-organized molecular machines," *Phys. Rev. E*, vol. 49, no. 6, p. 5462, 1994.

[48] D. Beysens, G. Forgacs, and J. Glazier, "Cell sorting is analogous to phase ordering in fluids," *PNAS*, vol. 97, no. 17, pp. 9467–9471, 2000.

[49] D. Chandler, *Introduction to Modern Statistical Mechanics*. Oxford University Press, 1987.

[50] P. Panorchan, M. S. Thompson, K. J. Davis, Y. Tseng, K. Konstantopoulos, and D. Wirtz, "Single-molecule analysis of cadherin-mediated cell-cell adhesion," *J. Cell Sci.*, vol. 119, no. 1, pp. 66–74, 2006.

[51] A. Gerisch and M. Chaplain, "Mathematical modelling of cancer cell invasion of tissue: local and non-local models and the effect of adhesion," *J. Theor. Biol.*, vol. 250, no. 4, pp. 684–704, 2008.

[52] A. Brú, J. M. Pastor, I. Fernaud, I. Brú, S. Melle, and C. Berenguer, "Super-rough dynamics on tumor growth," *Phys. Rev. Lett.*, vol. 81, no. 18, p. 4008, 1998.

[53] M. L. Mansfield and L. I. Klushin, "Monte carlo studies of dendrimer macromolecules," *Macromolecules*, vol. 26, no. 16, pp. 4262–4268, 1993.

[54] J. T. Bosko, B. Todd, and R. J. Sadus, "Analysis of the shape of dendrimers under shear," *J. Chem. Phys.*, vol. 124, p. 044910, 2006.

[55] H. Byrne and D. Drasdo, "Individual-based and continuum models of growing cell populations: a comparison," *J. math. biol.*, vol. 58, no. 4-5, pp. 657–687, 2009.

[56] H. Vodopick, E. Rupp, C. Edwards, F. Goswitz, and J. Beauchamp, "Spontaneous cyclic leukocytosis and thrombocytosis in chronic granulocytic leukemia," *New Engl. J. Med.*, vol. 286, no. 6, pp. 284–290, 1972.

[57] B. J. Kennedy, "Cyclic leukocyte oscillations in chronic myelogenous leukemia during hydroxyurea therapy," *Blood*, vol. 35, pp. 751–760, 1970.